Research Square

Preprints are preliminary reports that have not undergone peer review.
They should not be considered conclusive, used to inform clinical practice,
or referenced by the media as validated information.

VPS34-Mediated Autophagic Flux Supports γδ T Cell Survival and Anti-Tumor Immunity by Preserving Metabolic and Iron Homeostasis

Meixiang Yang

mxyang@jnu.edu.cn

Jinan University https://orcid.org/0000-0003-4547-3170

Jiamin Fu

Jinan University

Peiran Feng

Jinan University

Zerong Guan

Jun He

Jinan University

Hanlin Shuai

The Fifth Affiliated Hospital of Jinan University

Bihui Guo

Huizhou Second Maternal and Child Health Hospital

Bing Xin

Peking University Shenzhen Hospital https://orcid.org/0000-0002-8644-2429

Jiacong Yan

1Department of Reproductive Medicine, NHC Key Laboratory of Healthy Birth and Birth Defect Prevention in Western China, First People's Hospital of Yunnan Province, Kunming 650500, China 2Firs

Article

Keywords: γδ T cells, VPS34, Autophagic flux, Metabolic homeostasis, Iron homeostasis, Anti-tumor immunity

Posted Date: November 9th, 2026

DOI: https://doi.org/10.21203/rs.3.rs-11377148/v1

License: This work is licensed under a Creative Commons Attribution 4.0 International License.
Read Full License

Additional Declarations: (Not answered)

VPS34-Mediated Autophagic Flux Supports γδ T Cell Survival and Anti-Tumor Immunity by Preserving Metabolic and Iron Homeostasis

Jiamin Fu[1,2*], Peiran Feng[3*], Zerong Guan[4*], Bing Xin[5*], Jun He[6], Bihui Guo[7], Hanlin Shuai[1], Jiacong Yan[8,9#], Meixiang Yang[1,2,3,4,6#]

[1]The Fifth Affiliated Hospital of Jinan University (Heyuan Shenhe People's Hospital), Jinan University, Heyuan, 517000, China

[2]The Affiliated Guangdong Second Provincial General Hospital of Jinan University, Jinan University, Guangzhou, 510290, China

[3]Department of Orthopedic Surgery, The Sixth Affiliated Hospital of Jinan University (Dongguan), Dongguan, 523573, China

[4]State Key Laboratory of Bioactive Molecules and Druggability Assessment, The Biomedical Translational Research Institute, Health Science Center (School of Medicine), Jinan University, Guangzhou, 510632, China

[5]Peking University Shenzhen Hospital, Department of Pathology, Shenzhen Peking University-The Hong Kong University of Science and Technology Medical Center, Guangdong Province, 518036, China

[6]Key Laboratory of Ministry of Education for Viral Pathogenesis & Infection Prevention and Control (Jinan University). Guangzhou Key Laboratory for Germ-free animals and Microbiota Application. Institute of Laboratory Animal Science. School of Medicine. Jinan University. Guangzhou, 510632, China

[7]Department of Obstetrics and Gynecology, Huizhou Second Maternal and Child Health Hospital, Huizhou, 516003, China

[8]Department of Reproductive Medicine, NHC Key Laboratory of Healthy Birth and Birth Defect Prevention in Western China, First People's Hospital of Yunnan Province, Kunming, 650500, China

[9]KUST-YPFPH Reproductive Medicine Joint Research Center, Kunming, 650500, China

[*]These authors contributed equally to this work

Running title: VPS34 regulates γδ T cells viability and function

[#]Corresponding author:

Dr. Jiacong Yan, yan_jiacong@kust.edu.cn; Dr. Meixiang Yang, mxyang@jnu.edu.cn.

ABSTRACT

γδ T cells serve as key effectors of immune surveillance, and their survival and effector functions are tightly governed by precise metabolic regulation. However, the molecular mechanisms orchestrating metabolic homeostasis in γδ T cells remain incompletely defined. Here, we demonstrate that VPS34 is an indispensable regulator of γδ T cell development, peripheral homeostasis, and anti-tumor immunity by maintaining intact autophagic flux. Using LC3 dual-fluorescence reporter mice, we observed peak autophagic activity at the thymic DN stage, with intrinsically higher basal autophagy in thymic and peripheral γδ T cells compared with αβ T cells. T-cell-specific VPS34 deletion disrupts autophagic turnover and causes accumulation of LC3B, p62 and autophagosomes. While VPS34 ablation perturbs the shared DN3-to-DN4 thymic checkpoint for αβ and γδ T progenitors, peripheral $CD44^{hi}$ effector γδ T cells are selectively vulnerable to VPS34 loss. VPS34-deficient γδ T cells show impaired terminal maturation, skewed TCRγ usage, and reduced numbers across lymphoid and barrier tissues. Mechanistically, VPS34 deletion induces mitochondrial dysfunction and metabolic reprogramming in γδ T cells, accompanied by cellular iron overload, elevated CD71 and CD36 expression, and excessive mitochondrial and lipid-derived ROS. The resultant oxidative stress drives concurrent ferroptosis and apoptotic cell death. Both genetic and pharmacological VPS34 inhibition reprograms γδ T cell cytokine responses, dampening IFN-γ while boosting IL-17A production, and compromises γδ T-cell-mediated anti-tumor protection in melanoma adoptive-transfer models. Supporting these observations, metformin-driven autophagy augmentation elevates IFN-γ production and boosts anti-tumor activity in WT γδ T cells. Our findings illustrate how VPS34-dependent autophagy maintains γδ T cell fitness and anti-tumor immunity via coordinated control of metabolism and iron homeostasis, providing mechanistic insights for future γδ T-cell-based immunotherapeutic development.

Keywords: γδ T cells, VPS34, Autophagic flux, Metabolic homeostasis, Iron homeostasis, Anti-tumor immunity

INTRODUCTION

γδ T cells constitute an evolutionarily conserved innate-like lineage of unconventional T lymphocytes that bridge innate and adaptive immunity[1-3]. Their multifaceted roles in immune surveillance, pathogen clearance, tumor immunosurveillance, and autoimmune disease pathogenesis have attracted considerable research attention[4-6]. Unlike conventional αβ T cells, which require MHC-restricted antigen recognition for activation, γδ T cells initiate rapid, MHC-unrestricted effector responses through secretion of proinflammatory cytokines (e.g., IFN-γ, TNF-α) and direct cytotoxicity toward transformed or pathogen-infected host cells[7]. These distinctive properties render γδ T cells highly promising candidates for adoptive cellular immunotherapy against cancer, infectious diseases, and autoimmune disorders[6, 8]. γδ T cells originate from $CD4^{-}CD8^{-}$ double-negative (DN) thymic precursors and undergo ordered rearrangement of TCRγ and TCRδ chains within the thymic microenvironment. This tightly orchestrated developmental program governs γδ T cells lineage commitment, subset specification, and functional polarization[9]. Following thymic maturation, γδ T cells further differentiate into functionally specialized subsets with discrete effector programs. IFN-γ-producing γδ T cells predominantly mediate antitumor immunity, whereas IL-17A-producing subsets primarily drive antifungal defense and pathological inflammation[10-12]. Despite their considerable therapeutic potential, the intrinsic regulatory networks governing γδ T cell development, metabolic fitness, and effector polarization remain incompletely understood.

Autophagy is an evolutionarily conserved lysosomal degradation pathway that sustains lymphocyte homeostasis under metabolic stress by clearing damaged organelles, aggregated proteins, and toxic metabolites[13]. Functional autophagic flux is indispensable for thymocyte maturation, peripheral T cell survival, and innate lymphoid cell function[14-16]. Vacuolar protein sorting 34 (VPS34), encoded by *Pik3c3*, is the sole class III phosphatidylinositol 3-kinase (class III PI3K) and serves as a core upstream regulator of autophagosome biogenesis and autophagosome-lysosome fusion. Two distinct VPS34-containing complexes selectively drive autophagy initiation versus endolysosomal trafficking, thereby sustaining complete autophagic turnover[17]. Beyond its well-established roles in tumor biology[18-20], VPS34 has emerged as a critical

immune regulator that controls the development, survival, and activation of αβ T cells[21], regulatory T cells[22], macrophages[23], dendritic cells[24], and NK cells[25]. Notably, lymphocyte homeostasis and metabolic fitness are tightly coupled to VPS34-dependent autophagy[26]. However, existing investigations into the immunomodulatory functions of VPS34 have focused exclusively on αβ-lineage cells, and whether VPS34-governed autophagic flux regulates γδ T cell biology remains entirely unexplored.

In this study, we first mapped stage-specific autophagic dynamics across thymic γδ T cell development and confirmed that autophagic flux remains functionally active throughout γδ T cell development and maturation. Mature γδ T cells exhibit higher basal autophagic flux than αβ T cells. To dissect the functional requirement for VPS34 in this process, we generated *CD2-Cre*-mediated T cell-specific *Pik3c3* conditional knockout mice to systematically examine VPS34-mediated autophagic signaling in γδ T cells. Using both genetic ablation and pharmacological inhibition of VPS34, we demonstrate that VPS34 deficiency blocks autophagosome-lysosome fusion, impairs thymic γδ T cell maturation, and skews the peripheral TCRγ repertoire across lymphoid and barrier tissues. Mechanistically, we uncover a cascade in which defective VPS34-dependent autophagy triggers mitochondrial dysfunction, metabolic rewiring, iron and lipid dyshomeostasis, excessive ROS accumulation, and concomitant ferroptosis and apoptosis, leading to selective depletion of cytotoxic $CD44^{hi}$ effector γδ T cells. Functionally, we establish that VPS34 is required for IFN-γ-dominant antitumor polarization of γδ T cells. Collectively, our findings demonstrate that VPS34-dependent autophagy sustains γδ T cell homeostasis and anti-tumor effector fitness by preserving metabolic and iron homeostasis. This work expands our understanding of γδ T cell regulation and suggests that VPS34 activity may represent a relevant consideration for refining γδ T cell-based immunotherapies.

RESULTS

Autophagic flux is functionally active during γδ T cell development and maturation

To examine whether autophagy is dynamically regulated throughout γδ T cell development, we profiled autophagic activity across successive thymocyte developmental stages using *CAG-RFP-EGFP-LC3* reporter mice. This reporter system enables real-time visualization and quantification of autophagosome dynamics via

expression of LC3 fused to RFP and EGFP. Briefly, $EGFP^+$ RFP^+ puncta represent intact autophagosomes, where both fluorophores remain stable within the neutral autophagosomal lumen. $EGFP^-RFP^+$ puncta correspond to autolysosomes, as EGFP fluorescence is quenched in the acidic lysosomal compartment (Figure S1A). Flow cytometry revealed substantial autophagic flux across major thymocyte subsets, including double-negative (DN; $CD4^-CD8^-$), double-positive (DP; $CD4^+CD8^+$), and $CD4^+$ or $CD8^+$ single-positive (SP) thymocytes (Figure 1A, B). DN thymocytes showed the highest autophagic activity, with significantly higher frequencies of $EGFP^+RFP^+$ and $EGFP^-RFP^+$ cells relative to other thymocyte populations (Figure 1A, B). To validate these observations at the protein level, we performed intracellular flow cytometry for LC3B, a core autophagosome marker, on wild-type (WT) thymocytes. Among major thymocyte subsets, DN thymocytes displayed the highest LC3B mean fluorescence intensity (MFI) (Figure 1C). We further measured autophagosome abundance using an autophagosome-specific fluorescent probe. Consistent with the LC3B data, DN thymocytes had the highest autophagosome-probe MFI of all thymic populations (Figure 1D). Collectively, these data demonstrate functional autophagic flux during early thymocyte development, with peak LC3B expression and autophagosome accumulation occurring at the DN stage, a critical checkpoint for γδ T cell lineage specification.

To confirm that these autophagosome-associated signals reflect functional autophagic flux rather than static accumulation, we treated primary thymocytes from *CAG-RFP-EGFP-LC3* reporter mice with bafilomycin A1 (BafA1). BafA1 inhibits vacuolar H^+-ATPase, suppresses lysosomal acidification, and blocks autophagic turnover. Following BafA1 exposure, we observed a marked increase in the frequency of $EGFP^+RFP^+$ cells across all major thymocyte subsets (Figure 1E, F). This effect was most pronounced in DN thymocytes, which showed robust autophagosome accumulation upon BafA1 treatment (Figure 1E, F). These findings indicate that high autophagic activity in early thymocytes stems from continuous autophagosome formation and lysosomal degradation, confirming functional autophagic flux during the developmental window for γδ T cell lineage commitment.

After TCR rearrangement, thymocytes commit to either the αβ or γδ T-cell lineage. We next asked whether lineage specification is accompanied by intrinsic differences in basal

autophagic activity. We compared autophagic flux between thymic γδ T cells ($CD3^+TCR\gamma\delta^+$) and αβ T cells ($CD3^+TCR\gamma\delta^-$) isolated from *CAG-RFP-EGFP-LC3* reporter mice. Thymic γδ T cells contained significantly higher fractions of $EGFP^+RFP^+$ and $EGFP^-RFP^+$ cells than αβ T counterparts, pointing to higher autophagic flux within the γδ T-cell lineage (Figure 1G, H). In agreement with this result, both LC3B MFI and autophagosome probe signals were substantially higher in thymic γδ T cells (Figure 1I, J). BafA1 treatment triggered clear accumulation of $EGFP^+RFP^+$ autophagosomes in thymic γδ T cells (Figure 1K), verifying active autophagosome synthesis and turnover under homeostatic conditions.

Upon exiting the thymus, mature γδ T cells traffic to secondary lymphoid organs to carry out effector functions. We therefore assessed autophagic activity in peripheral γδ T cells from *CAG-RFP-EGFP-LC3* reporter mice. Splenic WT γδ T cells exhibited high proportions of $EGFP^+RFP^+$ and $EGFP^-RFP^+$ puncta-positive events, consistent with intact autophagic flux (Figure S1B, C). At the protein level, splenic γδ T cells had significantly higher LC3B MFI and autophagosome probe signals than splenic αβ T cells (Figure S1D, E). BafA1 treatment increased $EGFP^+RFP^+$ frequencies among splenic γδ T cells (Figure 1L), confirming basal autophagic flux in mature peripheral γδ T cells. Taken together, our results define stage- and lineage-dependent autophagic regulation during T-cell thymic development. Autophagic flux peaks at the DN stage of early thymopoiesis and remains constitutively higher in lineage-committed and mature γδ T cells, suggesting autophagy may support γδ T-cell lineage specification and homeostasis.

VPS34 deficiency disrupts autophagic flux in γδ T cells

VPS34, encoded by *Pik3c3*, is the sole class-III PI3-kinase in mammals and a central upstream regulator of autophagosome biogenesis and autophagic flux. To investigate the cell-intrinsic role of VPS34 in γδ T cell autophagy and to define the affected regulatory stage, we generated $Pik3c3^{fl/fl}CD2^{Cre}$ conditional knockout (cKO) mice by crossing loxP-flanked *Pik3c3* mice with $CD2^{Cre}$ transgenic mice, with $Pik3c3^{fl/fl}$ littermates serving as wild-type (WT) controls. $CD2^{Cre}$ drives recombination specifically at the DN2/3 stage of thymocyte development, enabling targeted VPS34 deletion in developing γδ T cells for subsequent autophagy assays (Figure S2A). Quantitative real-time PCR confirmed efficient *Pik3c3* deletion, with *Pik3c3* mRNA nearly undetectable in cKO thymocytes

relative to WT littermates (Figure S2B). We next profiled autophagy-related markers in $CD3^+TCR\gamma\delta^+$ γδ T cells by intracellular flow cytometry, given the limited numbers of primary γδ T cells available for biochemical assays. Relative to WT γδ T cells, VPS34-deficient γδ T cells showed elevated levels of LC3B and the autophagy adaptor p62 (SQSTM1) (Figure 2A, B), alongside marked accumulation of autophagosome-probe signal (Figure 2C). These data indicate that VPS34 is required for normal autophagic flux in γδ T cells.

To confirm these autophagy defects result specifically from VPS34 loss, we treated primary WT γδ T cells for 24 h with the selective VPS34 inhibitor VPS34-IN-1 (5 μM). DMSO-treated cells served as vehicle controls. Immunoblot analysis showed that VPS34-IN-1 increased the LC3-II and p62 protein abundance relative to DMSO (Figure 2D, E). Of note, a higher LC3-II and autophagosome accumulation can arise either from enhanced autophagy initiation or from impaired turnover after autophagosome formation. To distinguish these possibilities, we added BafA1 to block lysosomal degradation. In DMSO-treated cells, BafA1 caused robust accumulation of LC3-II and p62, demonstrating active autophagic flux. In VPS34-IN-1-treated cells, however, BafA1 produced no further increase in LC3-II or p62 (Figure 2D, E). The absence of additive accumulation suggests VPS34 acts upstream of lysosomal-acidification-dependent autophagic turnover, rather than primarily controlling autophagosome biogenesis itself.

We repeated this experiment using γδ T cells purified from *CAG-RFP-EGFP-LC3* reporter mice as an independent readout. Cells were pretreated for 24 h with VPS34-IN-1 or DMSO, then exposed to BafA1 for an additional 4 h. Consistent with our cKO observations, VPS34-IN-1-pretreated cells displayed higher basal $EGFP^+RFP^+$ frequency and lower $EGFP^-RFP^+$ frequency compared with DMSO controls (Figure 2F, G). Moreover, BafA1 failed to further increase $EGFP^+RFP^+$ proportions in inhibitor-pretreated γδ T cells (Figure 2F, G). These in-vitro pharmacological results recapitulate our genetic-deletion data and reinforce that VPS34 is necessary to sustain complete autophagic flux in γδ T cells.

VPS34 deficiency impairs γδ T cell thymic development and maturation

Having established that VPS34 supports autophagic flux in γδ T cells, we next examined whether VPS34 deficiency affects thymic γδ T cell development and maturation. In line

with published roles for VPS34 in thymocyte homeostasis, *Pik3c3*$^{fl/fl}$*CD2*^{Cre} cKO mice exhibited obvious thymic hypoplasia compared with *Pik3c3*$^{fl/fl}$ littermates; both thymus weight and total thymocyte counts were significantly reduced (Figure 3A, B). We used CD4 and CD8 surface staining to map developmental blocks. VPS34-deficient thymi contained fewer double-positive (DP; $CD4^+CD8^+$) and single-positive (SP; $CD4^+$ or $CD8^+$) thymocytes, with a concomitant relative expansion of the double-negative (DN; $CD4^-CD8^-$) compartment (Figure 3C). Further subdivision of the DN pool, where γδ T-cell lineage commitment occurs, revealed an increased frequency of DN3 ($CD44^-CD25^+$) thymocytes and a corresponding reduction in DN4 ($CD44^-CD25^-$) cells (Figure 3D), pointing to a developmental arrest at the β-selection checkpoint. In keeping with this arrest, DN thymocytes from cKO mice had higher CD25 surface expression (Figure 3E). Peripheral lymph-node and spleen αβ T-cell numbers were also strongly diminished in cKO animals (Figure S3A-C), confirming broad impairment of T-cell development upon VPS34 ablation.

Because γδ T-cell lineage commitment takes place within the DN window, the same window when *CD2*^{Cre}-driven deletion occurs and autophagic flux peaks, we focused next on thymic γδ T-cell development. Total thymic γδ T-cell ($CD3^+TCR\gamma\delta^+$) absolute numbers were markedly lower in cKO mice than WT littermates (Figure 3F). To dissect stage-specific maturation defects, we used CD24 and CD73, markers tracking γδ T-cell commitment and terminal maturation. γδ T-cell maturation proceeds sequentially through uncommitted ($CD24^+CD73^-$), lineage-committed ($CD24^+CD73^+$), and terminally mature ($CD24^-CD73^+$) stages; CD73 acquisition marks definitive γδ-lineage commitment[27, 28]. Loss of VPS34 did not substantially change the frequency of uncommitted $CD24^+CD73^-$ precursors. The proportion of committed $CD24^+CD73^+$ cells increased moderately, whereas terminally mature $CD24^-CD73^+$ γδ T cells were significantly reduced (Figure 3G). These results suggest VPS34-dependent autophagy contributes to terminal maturation of thymic γδ T cells.

We next examined TCRγ chain usage, which shapes subset identity and functional properties. TCR-repertoire analysis showed subset skewing in VPS34-deficient mice. $V\gamma4^+$ γδ T cells were reduced, whereas the relative proportion of $V\gamma1^+$ cells increased compared with WT controls (Figure 3H). Within each major subset ($V\gamma1^+$, $V\gamma4^+$,

253 Vγ1^{-}Vγ4^{-}), the frequency of terminally mature CD24^{-}CD73^{+} cells was lower in cKO
254 mice (Figure 3I-K). Collectively, these data demonstrate that VPS34 is required for
255 terminal maturation and normal TCRγ-repertoire homeostasis among thymic γδ T cells.
256 **VPS34 deficiency disrupts peripheral γδ T cell homeostasis and tissue distribution**
257 We then evaluated peripheral γδ T-cell homeostasis, subset composition, and tissue
258 distribution in VPS34-deficient animals. Flow-cytometry analysis of CD3^{+}TCRγδ^{+} cells
259 in spleen and lymph nodes showed significantly reduced absolute γδ T-cell numbers in
260 *Pik3c3$^{fl/fl}$CD2^{Cre}* mice relative to littermate controls (Figure 4A). Notably, the subset
261 skewing observed in the thymus, reduced Vγ4^{+} populations and expanded Vγ1^{+} subsets,
262 was also evident in these peripheral lymphoid tissues (Figure 4B, C). To test whether
263 these peripheral defects reflect cell-intrinsic VPS34 requirements, we set up competitive
264 bone-marrow (BM) chimeras. Irradiated CD45.1^{+}CD45.2^{+} recipient mice were
265 reconstituted with a 1:1 mixture of CD45.1^{+} WT and CD45.2^{+} VPS34-deficient BM
266 progenitors (Figure 4D). This experimental setup permits direct side-by-side comparison
267 of WT and VPS34-deficient γδ T cells sharing identical in-vivo microenvironments. In
268 both spleen and lymph nodes, VPS34-deficient (CD45.2^{+}) γδ T cells contributed far less
269 to the total γδ T-cell pool than their WT (CD45.1^{+}) counterparts (Figure 4E). This
270 confirms a cell-autonomous requirement for VPS34 in maintaining peripheral γδ T-cell
271 homeostasis.
272 Beyond secondary lymphoid organs, we next investigated whether tissue-resident γδ T
273 cells in barrier and parenchymal tissues are similarly dependent on VPS34. We first
274 assessed autophagic flux in tissue-resident γδ T cells from barrier and parenchymal tissues
275 (skin, cLP, small intestine, liver, and lung) of *CAG-RFP-EGFP-LC3* reporter mice by
276 flow cytometry. Tissue-resident γδ T cells from all examined tissues showed measurable
277 autophagic flux, with readily detectable EGFP^{+}RFP^{+} autophagosome and EGFP^{-}RFP^{+}
278 autolysosome populations (Figure S4A). Thus tissue-resident γδ T cells maintain
279 constitutive autophagic activity under homeostatic conditions. We next enumerated γδ T
280 cells across these tissues and found consistent numerical reductions in VPS34-deficient
281 mice (Figure 4F, G). Given the importance of γδ T cells in skin physiology, we further
282 separated skin-resident γδ T cells into epidermal and dermal subsets. Both epidermal and
283 dermal γδ T-cell populations were significantly depleted in frequency and absolute

number in cKO animals (Figure 4H, I). Collectively, these findings demonstrate that VPS34-dependent autophagy is required to maintain γδ T cell homeostasis and tissue distribution across multiple anatomical sites.

VPS34 deficiency induces mitochondrial dysfunction, metabolic reprogramming and ROS accumulation in γδ T cells

Autophagy mediates clearance of damaged mitochondria, and autophagy impairment results in accumulation of dysfunctional mitochondria[29]. We therefore assessed mitochondrial homeostasis in γδ T cells from cKO and WT mice. VPS34-deficient γδ T cells exhibited increased mitochondrial mass and elevated mitochondrial membrane potential, both signatures of dysfunctional mitochondria accumulating due to defective autophagic turnover (Figure 5A, B). Mitochondria govern core immune-cell metabolism, balancing oxidative phosphorylation and glycolysis[30]. To quantify single-cell metabolic perturbations, we employed SCENITH (Single-cell Metabolism by Analysis of Translation Inhibition)[31], a flow cytometry-based assay for resolving cellular metabolic dependencies. Comparison of γδ T cells purified from *Pik3c3*$^{fl/fl}$*CD2*^{Cre} cKO and *Pik3c3*$^{fl/fl}$ WT mice revealed profound metabolic reprogramming upon VPS34 deletion. VPS34-deficient γδ T cells shifted away from a quiescent metabolic baseline toward greater reliance on mitochondrial oxidative metabolism, accompanied by reduced glycolytic capacity (Figure 5C). Consistent with this hypermetabolic state, VPS34-deficient γδ T cells expressed higher Ki-67 (marker of cellular proliferation), and displayed increased cell size and granularity (Figure 5D, E). These data indicate that mitochondrial dysfunction-driven metabolic activation disrupts the quiescent state of VPS34-deficient γδ T cells.

Damaged mitochondria constitute a major source of intracellular reactive oxygen species (ROS). We detected significantly higher total ROS and mitochondrial-derived ROS in VPS34-deficient γδ T cells relative to WT controls (Figure 5F, G). Excess ROS compromises cell viability; accordingly, we observed an increased fraction of 7-AAD^{+} dying cells among VPS34-deficient γδ T cells (Figure 5H). To establish a functional link between ROS excess and reduced viability, we treated WT and cKO γδ T cells with the ROS scavenger N-acetyl-L-cysteine (NAC). NAC treatment lowered intracellular ROS (Figure 5I) and significantly rescued the viability defect of VPS34-deficient γδ T cells

(Figure 5J). Collectively, these results outline a stress cascade triggered by VPS34 loss. Defective autophagic turnover leads to accumulation of dysfunctional mitochondria, which drives metabolic reprogramming and excessive ROS production, ultimately impairing γδ T-cell survival.

VPS34 deficiency compromises iron and lipid homeostasis and concurrent ferroptosis and apoptosis in γδ T cells

Mitochondrial dysfunction and excessive ROS production are critical upstream triggers of multiple cell death programs[32]. We next sought to define the cell-death mechanisms responsible for γδ T-cell loss in VPS34-deficient mice. Mitochondrial respiratory chain dysfunction facilitates lipid peroxidation, a core initiating event of ferroptosis, while intracellular iron overload further exacerbates lipid peroxide accumulation and ferroptotic progression[33]. We first detected key indicators governing iron and lipid metabolism. VPS34-deficient γδ T cells exhibited significantly increased intracellular iron levels compared with WT cells (Figure 6A). Transferrin receptor 1 (CD71), the major mediator of cellular iron uptake, was markedly upregulated in VPS34-deficient γδ T cells, suggesting enhanced iron acquisition (Figure 6B). CD36, a scavenger receptor that imports polyunsaturated fatty acids and facilitates lipid peroxidation, was also increased in cKO γδ T cells (Figure 6C). Consistent with disrupted iron-lipid homeostasis, lipid ROS accumulation was markedly higher in VPS34-deficient γδ T cells (Figure 6D). To test the contribution of ferroptosis, we used the specific inhibitor Ferrostatin-1 (Fer-1). Fer-1 treatment significantly improved the viability of VPS34-deficient γδ T cells (Figure 6E), demonstrating ferroptosis as an important driver of cell loss under VPS34 deficiency.

Beyond ferroptosis, persistent mitochondrial damage and ROS overload also activate intrinsic apoptotic signaling. Flow cytometry detected more Annexin V-positive apoptotic γδ T cells in $Pik3c3^{fl/fl}CD2^{Cre}$ mice (Figure 6F). At the molecular level, VPS34-deficient γδ T cells showed increased cleaved-Caspase-3 and elevated pro-apoptotic Bim protein, two central mediators of the intrinsic apoptotic cascade (Figure 6G, H). Pharmacological apoptosis inhibition with Z-VAD-FMK also partially restored survival of VPS34-deficient γδ T cells (Figure 6I). Notably, combined Fer-1 plus Z-VAD-FMK treatment produced additive protective effects compared with single-agent treatment (Figure 6I). This indicated that ferroptosis and apoptosis operate independently

and together eliminate VPS34-deficient γδ T cells. In summary, VPS34 deficiency disturbs iron and lipid homeostasis in γδ T cells, triggering concurrent ferroptotic and apoptotic death and driving net γδ T-cell loss.

VPS34 deficiency disrupts the homeostasis of effector γδ T cells

Within secondary lymphoid organs, peripheral γδ T cells can be subdivided by CD44/CD62L into naïve $CD44^{lo}CD62L^{hi}$ and effector $CD44^{hi}CD62L^{lo}$ subsets[34]. Effector-phenotype γδ T cells arise from naïve precursors following antigen-driven differentiation and represent the main cytotoxic population mediating anti-pathogen and anti-tumor immunity. Using *CAG-RFP-EGFP-LC3* reporter mice, we compared basal autophagic flux between naïve and effector γδ T-cell subsets. Effector γδ T cells contained significantly higher frequencies of both $EGFP^{+}RFP^{+}$ autophagosome-positive and $EGFP^{-}RFP^{+}$ autolysosome-positive events than naïve γδ T cells (Figure S5A, B), indicating intrinsically higher basal autophagic flux in effector γδ T cells.

We next tested whether this elevated autophagic flux depends on VPS34 catalytic activity. WT effector γδ T cells were cultured for 24 h with VPS34-IN-1 or DMSO vehicle. VPS34-IN-1 exposure increased the frequency of $EGFP^{+}RFP^{+}$ autophagosome-positive cells relative to DMSO controls, consistent with impaired autophagosome maturation (Figure S5C, D). BafA1 addition further accumulated autophagosomes in DMSO-treated cells, yet produced no additional increase in VPS34-IN-1-pretreated effector γδ T cells (Figure S5C, D). The lack of BafA1-responsive autophagosome buildup indicates VPS34 catalytic function is required to sustain complete autophagic flux in effector γδ T cells.

We then assessed the in-vivo consequences of VPS34 loss for effector-subset maintenance. In $Pik3c3^{fl/fl}CD2^{Cre}$ mice, the frequency of $CD44^{hi}CD62L^{lo}$ effector γδ T cells was substantially reduced compared with $Pik3c3^{fl/fl}$ littermates, accompanied by a reciprocal expansion of $CD44^{lo}CD62L^{hi}$ naïve γδ T cells (Figure 7A, B). To determine if this skewing is cell-intrinsic, we generated competitive BM chimeras by transferring a 1:1 mixture of $CD45.1^{+}$ WT and $CD45.2^{+}$ VPS34-deficient BM progenitors into irradiated recipients. Within the same host, VPS34-deficient γδ T cells were under-represented among the effector pool, whereas the naïve subset was largely preserved (Figure S6A, B). This establishes cell-autonomous VPS34 dependence for effector γδ T-cell maintenance.

Given this selective effector-subset loss, we examined cell survival in subset-gated populations. VPS34-deficient $CD44^{hi}$ effector γδ T cells showed greatly increased Annexin V^+ and 7-AAD^+ fractions compared with WT counterparts. In contrast, $CD44^{lo}$ naïve γδ T cells showed only modest changes in cell-death markers (Figure 7C, D). These data confirm that effector γδ T cells are selectively vulnerable to VPS34 loss. We further characterized effector-subset metabolic defects. VPS34-deficient $CD44^{hi}$ effector γδ T cells displayed higher mitochondrial mass and mitochondrial-membrane hyperpolarization (Figure 7E, F), alongside elevated total cellular ROS, mitochondrial ROS, and lipid peroxidation (Figure 7G-I). Collectively these findings demonstrate that VPS34 sustains constitutive autophagic flux in effector γδ T cells. Loss of VPS34 results in mitochondrial dysfunction, excessive ROS generation, and increased lipid peroxidation within this subset.

VPS34-dependent autophagy restrains pro-inflammatory polarization and sustains anti-tumor function of γδ T cells

γδ T cells recognize target antigens in an MHC-independent manner and execute diverse immune functions via the production of signature effector cytokines[5]. To explore how VPS34-dependent autophagy shapes γδ T-cell effector responses, we employed two established in-vivo models, including imiquimod (IMQ)-induced psoriatic inflammation and B16F0 melanoma tumor models. The IMQ model activates TCR signaling and engages the IL-23-STAT3-IL-17A axis, which drives pro-inflammatory γδ T-cell function during cutaneous inflammation[35]. In this inflammatory setting, γδ T cells isolated from draining lymph nodes of VPS34-deficient mice produced markedly more IL-17A than WT γδ T cells (Figure 8A). In the B16F0 melanoma model, tumor-infiltrating VPS34-deficient γδ T cells displayed altered cytokine profiles eleven days after tumor inoculation. IFN-γ (key mediator of γδ T-cell anti-tumor cytotoxicity) was reduced, while IL-17A secretion was enhanced (Figure 8B). To exclude confounding secondary developmental defects caused by lifelong VPS34 deletion, we acutely inhibited VPS34 in mature WT γδ T cells during in-vitro functional polarization. Short-term VPS34-IN-1 treatment reproduced the in-vivo functional shift. Activated γδ T cells showed suppressed IFN-γ and augmented IL-17A production (Figure 8C, D). These

results demonstrate that VPS34-dependent autophagy directly controls mature γδ T-cell cytokine polarization, independent of earlier developmental events.

Given the essential role of IFN-γ in γδ T cell-based tumor surveillance, we further evaluated whether VPS34 inhibition impairs γδ T cell anti-tumor activity. Ex-vivo expanded γδ T cells were pretreated with either VPS34-IN-1 or DMSO, then adoptively transferred into tumor-bearing *TCRδ*$^{-/-}$ mice. Mice receiving VPS34-IN-1-pretreated γδ T cells failed to constrain tumor growth effectively, showing accelerated tumor progression, larger tumor volumes, and heavier tumor weights relative to the vehicle group (Figure 8E-G). These data indicate basal VPS34-dependent autophagic signaling is essential to preserve the anti-tumor effector identity of γδ T cells and limit excessive pro-inflammatory polarization.

Pharmacological autophagy activation potentiates γδ T cell anti-tumor cytotoxicity

To further support the functional link between autophagic activity and γδ T-cell effector capacity, we pharmacologically induced autophagy using metformin, an AMPK agonist known to suppress mTORC1 and boost autophagic flux in immune cells[36]. Intracellular LC3B staining by flow cytometry showed that metformin treatment increased autophagic flux in mature γδ T cells (Figure 8H). Functionally, autophagy induction was accompanied by a significant enhancement of the anti-tumor effector functions. Metformin-conditioned γδ T cells displayed increased production of IFN-γ, a signature cytokine for tumor immune surveillance (Figure 8I). We next measured direct cytotoxicity by co-culturing γδ T cells with B16F0 melanoma targets across multiple effector-to-target (E:T) ratios. Metformin-pretreated γδ T cells exhibited substantially greater tumor-killing capacity at all tested E:T ratios, as reflected by reduced target-cell viability (Figure 8J, K).

We extended these in-vitro findings to a pre-clinical adoptive-transfer tumor model using *Rag2*$^{-/-}$ mice, which lack endogenous mature T and B lymphocytes. B16F0 tumor cells were inoculated subcutaneously, and tumor engraftment was confirmed prior to the initiation of γδ T cell adoptive transfer. WT γδ T cells were pre-cultured for 24 h with or without metformin, then administered by repeated intravenous infusion (Figure 8L). Consistent with in-vitro cytotoxicity data, mice receiving metformin-preconditioned γδ T cells exhibited slower tumor progression, with smaller tumor volumes and lower tumor

weights compared with animals given untreated γδ T cells (Figure 8M-O). Analysis of tumor-infiltrating γδ T cells further revealed higher intratumoral IFN-γ expression following metformin pre-treatment (Figure 8P). These results demonstrate that pharmacological autophagy enhancement via metformin strengthens γδ T-cell anti-tumor capacity, further supporting that intact autophagic flux is necessary for normal γδ T-cell anti-tumor function.

DISCUSSION

Autophagy controls immune cell development, organelle quality maintenance and metabolic homeostasis. While VPS34-dependent autophagy is well studied in conventional αβ T cells and Tregs, stage-specific autophagic dynamics during γδ T cell development remain unclear. Using LC3 dual-fluorescence reporter mice, we found autophagic flux peaks at the DN thymocyte stage and is intrinsically higher in thymic and peripheral γδ T cells relative to αβ T cells. We further showed that VPS34-dependent autophagy controls γδ T cell development, peripheral survival, metabolic homeostasis and anti-tumor polarization. VPS34 deletion blocks autophagic flux, disrupts mitochondrial and iron-lipid redox balance, reduces effector γδ T cell survival and redirects cytokine secretion from IFN-γ to IL-17A, impairing anti-tumor immunity. Supporting these loss-of-function results, metformin-mediated autophagy activation boosted IFN-γ production and anti-tumor activity of γδ T cells. Collectively, our experiments establish autophagy as an essential regulator sustaining γδ T cell survival and effector function, advancing our knowledge of immunometabolism in innate T cells.

By profiling autophagic dynamics throughout thymocyte development using LC3 dual-fluorescence reporter mice, we detected functionally active autophagic flux during early T cell development, with peak autophagic activity at the DN stage, a critical window for γδ T cell lineage specification. Inter-lineage comparison revealed that thymic and peripheral γδ T cells display higher basal autophagic flux than αβ T cells under physiological conditions, pointing to sustained autophagy activation during γδ T cell maturation and peripheral maintenance. VPS34 is the sole class III PI3K in mammals and functions as an upstream master regulator of canonical autophagy, endosomal trafficking and lysosomal maturation. Prior work has demonstrated that T cells are highly sensitive

to perturbations in autophagy, with autophagy serving as a key regulator across distinct T cell subsets. In *CD4-Cre* and *Lck-Cre* mouse models, VPS34 deficiency reduces αβ T cell numbers and induces metabolic and differentiation defects[21, 37]. Our earlier work also established that VPS34 is essential for the survival and functional integrity of regulatory T cells (Tregs)[22]. Complementarily, Chi and colleagues showed that VPS34-dependent metabolic signaling shapes the transitional heterogeneity and maintenance of effector Tregs (eTregs), with these adaptations governing both autoimmune and anti-tumor immune responses[38]. Nevertheless, these investigations centered exclusively on adaptive T cell lineages and did not address the unique developmental and functional features of γδ T cells, including their thymus-primed effector commitment, rapid activation, and distinct metabolic requirements. Using *Pik3c3*$^{fl/fl}$*CD2*^{Cre} cKO conditional knockout mice, we found that VPS34 ablation impairs the DN3-to-DN4 transition and limits the progenitor-stage generation of both αβ and γδ T lineages. Despite this shared early thymic developmental block at the progenitor stage, marked phenotypic differences emerge between αβ and γδ T cell lineages in the periphery upon VPS34 deletion. Previous studies reported that VPS34 deficiency mainly impairs the survival of naïve αβ T cells[39]. In contrast, our results show that VPS34 loss selectively eliminates CD44^{hi} effector γδ T cells. This lineage- and subset-selective vulnerability reveals a unique requirement for VPS34-dependent autophagy to sustain effector γδ T cell maintenance. These findings connect the intrinsically elevated basal autophagic activity of γδ T cells to their effector homeostasis and developmental fitness. We propose that this phenotypic discrepancy arises from intrinsic developmental and metabolic differences between αβ and γδ T cells. Most peripheral γδ T cells, including IFN-γ$^+$ and IL-17A$^+$ subsets, acquire effector fates before exiting the thymus, resulting in a larger fraction of effector cells within the peripheral γδ T pool relative to αβ T cells[40]. Furthermore, the rapid TCR responsiveness of γδ T cells imposes high acute metabolic demand, which further increases their reliance on VPS34-mediated autophagy to preserve bioenergetic and homeostatic balance.

The inherent metabolic and effector priming status of γδ T cells renders them particularly dependent on constitutive autophagic activity to sustain intracellular quality control and redox stability. As rapidly responsive pre-committed effector cells, γδ T cells maintain high metabolic flux and baseline oxidative stress, creating a demand for

autophagy-supported mitochondrial quality control and metabolite recycling. In this context, VPS34 ablation substantially diminishes basal autophagic flux in γδ T cells, leading to defective mitochondrial quality surveillance. The inadequate autophagy-supported mitochondrial quality control results in accumulation of damaged mitochondria, mitochondrial hyperpolarization, and excessive ROS production, thereby disrupting intracellular redox homeostasis. In line with this metabolic deterioration, VPS34-deficient γδ T cells exhibit iron overload and enhanced lipid peroxidation, while compensatory CD71 upregulation further exacerbates iron accumulation, forming a persistent oxidative stress loop that drives effector cell death[41]. This mechanistic cascade explains the selective loss of effector γδ T subsets upon VPS34 deletion and establishes a direct link between developmentally programmed high autophagic flux, VPS34-dependent metabolic control, and peripheral effector γδ T cell survival. These observations extend previous models established in adaptive T cells and highlight a lineage-specific metabolic safeguard mechanism that is particularly critical for innate γδ T lymphocytes.

Beyond governing peripheral effector survival and metabolic homeostasis, VPS34-dependent autophagy also critically shapes the functional polarization of γδ T cells. Prior VPS34 studies in conventional αβ T cells mainly concentrated on thymic development and peripheral homeostasis maintenance. Although several studies have described VPS34-mediated functional regulation in regulatory T cells[22, 38], few reports have addressed its role in governing cytokine polarization and functional specification of innate γδ T cells. Our genetic and pharmacological evidence demonstrates that VPS34 insufficiency fundamentally alters γδ T cell functional identity, suppressing IFN-γ-mediated anti-tumor cytotoxicity while exaggerating IL-17A-associated pro-inflammatory programming. Given that high basal autophagic flux is a constitutive feature of developmentally primed γδ effector cells, autophagy impairment disrupts their innate effector transcriptional and metabolic programming. Unlike adaptive αβ T cells, which acquire effector functions post-antigen stimulation, γδ T cells rely on steady-state VPS34-autophagy to sustain their predominant anti-tumor effector profile and limit excessive pro-inflammatory IL-17A$^+$ polarization. This subset-specific functional regulation further distinguishes VPS34-autophagy functions in innate γδ T cells from

conventional T cell subsets.

To further validate the causal link between autophagic activity and γδ T cell anti-tumor function, we performed metformin-mediated autophagy activation assays. Metformin is a well-characterized metabolic activator that elevates cellular autophagic flux via canonical AMPK–mTORC1 signaling. Prior work has shown metformin can modulate γδ T cell function[42, 43], and our results further demonstrate that metformin treatment effectively enhances basal autophagic activity in wild-type γδ T cells. Functionally, autophagy augmentation significantly reinforces IFN-γ production and tumor-killing capacity of γδ T cells. In vivo adoptive transfer experiments further demonstrated that metformin-preconditioned γδ T cells exert superior anti-tumor efficacy and sustain elevated intratumoral IFN-γ expression. Collectively, these results fully support our genetic knockout findings, demonstrating that intact autophagic flux is required to maintain the anti-tumor effector competence of γδ T cells.

MATERIALS AND METHODS

Mice

Pik3c3$^{fl/fl}$, *CD2*^{Cre}, *CAG-RFP-EGFP-LC3* transgenic mice, CD45.1 congenic, *Rag2*$^{-/-}$ and *TCRδ*$^{-/-}$ mice were obtained from The Jackson Laboratory (Bar Harbor, ME, USA). VPS34 conditional knockout (cKO) mice (*Pik3c3*$^{fl/fl}$*CD2*^{Cre}) were generated by crossing *Pik3c3*$^{fl/fl}$ with *CD2*^{Cre} mice. Age- and sex-matched *Pik3c3*$^{fl/fl}$ littermates served as wild-type (WT) controls. Unless otherwise specified, 8-10-week-old male and female mice were utilized for all experiments. Mice were housed in a specific pathogen-free (SPF) facility at Jinan University, with controlled temperature, humidity and 12-h light/dark cycles, and provided with standard chow and water ad libitum. All animal procedures were performed in accordance with institutional animal care guidelines and approved by the Animal Ethics Committee of Jinan University.

Quantitative real-time PCR (qRT-PCR)

Total RNA was extracted from cells using TRIzol reagent (Invitrogen) and reverse-transcribed into cDNA using the PrimeScript™ RT Reagent Kit (Takara). qRT-PCR was performed on a Bio-Rad CFX Connect™ cycler using SYBR Green Master Mix (Takara). The following primer sequences were used: *Pik3c3* (F: 5'-

CATGTTTCGCCAAGGAATG-3'; R: 5'-GGGAGTTCTTGTAGGTTCAG-3'); *Gapdh* (F: 5'-CCAGCTTAGGTTCATCAGGT-3'; R: 5'-TTGATGGCAACAATCTCCAC-3'). Relative mRNA expression was calculated using the $2^{-\Delta\Delta Ct}$ method and normalized to the housekeeping gene *Gapdh*.

Flow cytometry

Flow cytometric analysis was performed on a Cytek Aurora™ analyzer (Cytek), and data were processed using FlowJo software (v10.8). The following fluorochrome-conjugated antibodies and staining reagents were used. Surface markers: CD3 (145-2C11), TCRβ (H57-597), TCRγδ (GL3), CD4 (GK1.5), CD8 (53-6.7), CD25 (PC-61), CD44 (1M7), CD62L (MEL-14), Vγ1.1/CR4 (2.11), Vγ2 (UC3-10A6), CD24 (M1/69), CD73 (TY/11.8), CD45 (30-F11), CD45.1 (A20), CD45.2 (104), CD71 (R17217), CD36 (HM36); Intracellular markers: IFN-γ (XMG1.2), IL-17A (TC11-18H10.1), Caspase-3 (C92-605) (BD Biosciences); Phosphoproteins & apoptosis: Bim (C34C5) (Cell Signaling Technology); ROS & mitochondrial function: MitoSOX Red (Invitrogen, Cat# M36008), CellROX Deep Red (Invitrogen, Cat# C10422), TMRM (Invitrogen, Cat# I34361), MitoTracker (Invitrogen, Cat# M22426); Iron metabolism: FerroOrange (Dojindo, Cat# F374); Lipid peroxidation: BODIPY 581/591 C11 (Thermo Fisher, Cat# D3861); Autophagy markers: LC3B (Novus Biologicals, Cat# NB100-2220), SQSTM1/p62 (Novus Biologicals, Cat# NBP1-48320). Live-cell kit-derived fluorescent probes: Autophagosome-selective Green Detection Reagent (Abcam, Autophagy Detection Kit, Cat# ab139484). FerroOrange, BODIPY 581/591 C11, and autophagosome-selective Green Detection Reagent were used for live-cell staining. Briefly, cells were incubated with corresponding probes following manufacturer-recommended concentration and incubation time at 37 °C prior to flow-cytometric acquisition. Intracellular staining for cleaved Caspase-3, Bim and anti-Puromycin was performed using the Foxp3/Transcription Factor Buffer Set (Thermo Fisher, Cat# 00-5523-00) according to the manufacturer's instructions.

Bone marrow chimeric mice

Donor WT ($CD45.1^+$) and $Pik3c3^{fl/fl}CD2^{Cre}$ ($CD45.2^+$) mice were intravenously injected with 150 mg/kg 5-fluorouracil (5-FU). Four days post-treatment, bone marrow (BM) cells were harvested by flushing femurs and tibias with sterile PBS, and red blood cells were

lysed with Red Blood Cell Lysis Buffer. WT ($CD45.1^+$) and $Pik3c3^{fl/fl}CD2^{Cre}$ ($CD45.2^+$) BM cells were mixed at a 1:1 ratio, and 1×10^7 mixed BM cells were intravenously transplanted into lethally irradiated (8 Gy) $CD45.1^+CD45.2^+$ recipient mice. Hematopoietic reconstitution and immune cell subsets were analyzed by flow cytometry 8 weeks after transplantation.

SCENITH analysis

Splenocytes were seeded in 96-well plates at 5×10^6 cells/mL, and pre-treated with the following reagents at 37°C with 5% CO_2 for 30 min: untreated control, 2-Deoxy-D-Glucose (DG, 200 mM, MedChemExpress, Cat# HY-13966), Oligomycin (Oligo, 2 μM, MedChemExpress, Cat# HY-16589), or 2-DG plus Oligomycin combination. Puromycin (10 μg/mL, MedChemExpress, Cat# HY-B1743A) was added for an additional 30 min to label nascent proteins. Cells were washed with ice-cold PBS, stained with fluorochrome-conjugated surface antibodies at 4°C for 20 min, then fixed and permeabilized using the Foxp3 Buffer Set. Intracellular puromycin was detected with anti-Puromycin antibody (12D10, Sigma-Aldrich, 1:100 dilution) at 4°C for 45 min. Flow cytometry was performed on a Cytek Aurora™ analyzer, and translational rates were calculated as previously described[44].

In vitro γδ T1/γδ T17 differentiation

48-well plates were pre-coated with purified anti-mouse γδ TCR antibody (UC7-13D5, 10 μg/mL, Bio X Cell) at 4°C overnight. Mouse splenocytes were seeded at 3.5×10^6 cells/mL in RPMI-1640 complete medium supplemented with 10% FBS and 1% pen-strep. For γδ T1 differentiation, cultures were supplemented with anti-CD28 (1 μg/mL) and anti-IL-2 neutralizing antibody (2 ng/mL). For γδ T17 differentiation, recombinant Recombinant murine IL-1β (10 ng/mL, PeproTech, Cat# 211-11B), Recombinant murine IL-23 (10 ng/mL, BioLegend, Cat# 589002) and Recombinant murine IFN-γ (10 μg/mL, PeproTech, Cat# 315-05-20UG) were additionally added. Cells were cultured at 37°C with 5% CO2; medium was refreshed on day 2 (i.e., on days 2 and 4), and cells were harvested on day 6. In selective experiments, VPS34-IN-1 (5 μM, MedChemExpress, Cat# HY-12795) was added to cultures 24 h prior to harvest. Total γδ T cells were enriched and analyzed by flow cytometry.

Western blotting

Cell samples were washed twice with ice-cold PBS (pH 7.4) and pelleted by centrifugation at 4 °C. Cell pellets were lysed on ice for 30 min in ice-cold RIPA buffer containing protease and phosphatase inhibitors, with brief vortexing every 10 min. Lysates were cleared by centrifugation at 4°C for 15 min, and supernatants were quantified using a BCA protein assay kit (Thermo Fisher Scientific). Equal-quantity protein samples were mixed with 5×SDS loading buffer, boiled at 95 °C for 10 min, and stored at -80 °C. Proteins and prestained molecular weight markers were resolved by 10% SDS-PAGE (80 V for stacking gel, 120 V for separation gel), followed by electro-transfer onto 0.45 μm PVDF membranes at 400 mA for 40 min. Membranes were blocked with 5% non-fat dry milk in TBST for 2 h at room temperature, and incubated overnight at 4°C with primary antibodies. After three 5-min TBST washes, membranes were probed with HRP-conjugated secondary antibodies for 1h at room temperature. Immunoreactive bands were visualized with enhanced chemiluminescence (ECL) and imaged using a ChemiDoc MP system (Bio-Rad).

Imiquimod-induced psoriasis mouse model

Eight-week-old female WT and cKO mice were depilated on the dorsal skin using depilatory cream (Veet) 24 h before the first application. Mice were topically treated with 62.5 mg of 5% imiquimod cream (Med-Shine Pharmaceutical, China) daily for 7 consecutive days on the depilated dorsal skin to induce psoriasis-like skin inflammation. On day 7, mice were euthanized, and draining inguinal and axillary lymph nodes were harvested. Intracellular staining and flow cytometry were performed to quantify IFN-γ and IL-17A production by γδ T cells.

B16F0 melanoma mouse model

For tumor growth assessment, WT and cKO mice were subcutaneously inoculated in the left flank with 3×10^5 B16F0 melanoma cells suspended in 100 μL sterile PBS. Mice were euthanized on day 11 post-inoculation, and tumors were harvested, minced, and mechanically dissociated through a 70-μm cell strainer. The resulting single-cell suspension was layered onto a 40% Percoll gradient and centrifuged at 400 × g for 20 min. Cells were collected, and treated with Red Blood Cell Lysis Buffer for 2–5 min at room temperature to remove red blood cells. After washing, tumor-infiltrating lymphocytes (TILs) were resuspended in FACS buffer and analyzed by flow cytometry.

For adoptive co-transfer experiments, ex vivo expanded γδ T cells were pretreated with 5 μM VPS34-IN-1 or DMSO vehicle for 24 h, then co-injected with B16F0 melanoma cells at a 1:4 ratio (γδ T cells: tumor cells) into *TCRδ*$^{-/-}$ mice. Tumor size was measured daily with a caliper, and tumor volume was calculated. Mice were sacrificed on day 20 post-injection; tumors were dissected, weighed and imaged for comparative analysis.

Effector-to-Target ratio analysis

Mouse splenocytes were prepared as single-cell suspensions in serum-free RPMI-1640 and counted. γδ T1 cells were differentiated and treated with metformin (0 or 10 μg/mL) for 24 h prior to harvest. B16F0 melanoma cells were trypsinized, centrifuged, and washed, then labeled with 10 μM CFSE in serum-free RPMI-1640 for 15 min at 37°C in the dark. Labeling was quenched with complete medium (10% FBS) for 10 min. Cells were centrifuged, washed 2–3 times to remove residual CFSE, and resuspended in R10F. CFSE-labeled B16F0 cells (1×10^4 cells/well) were co-cultured with γδ T cells in 96-well round-bottom plates at effector-to-target (E:T) ratios of 0:1, 5:1, 10:1, and 20:1 for 24 h at 37°C. Cells were then harvested and analyzed by flow cytometry for the percentage of $CFSE^{hi}$ $7AAD^+$ cells.

Adoptive transfer melanoma model in *Rag2*$^{-/-}$ mice

Rag2$^{-/-}$ mice (6–8 weeks old) were maintained under specific pathogen-free conditions. B16F0 melanoma cells (3×10^5 cells) were subcutaneously inoculated into the lower dorsal flank. After tumor engraftment was confirmed, mice were randomly assigned into three groups (n = 5 per group): (1) Control (PBS), (2) γδ T cells alone, and (3) Metformin + γδ T cells (Combination). γδ T cells were pre-treated ex vivo with or without metformin (10 μg/mL, MedChemExpress, Cat# HY-17471A) for 24 h. Then, 1×10^6 γδ T cells were intravenously infused into tumor-bearing recipients on days 0, 4, and 8. PBS control mice received an equal volume of PBS on a matching schedule. Tumor growth was monitored every 2 days by caliper measurement, and tumor volume was calculated as (length × width^2)/2. Mice were euthanized on day 12 after the first γδ T cell transfer, and tumor tissues were harvested for subsequent isolation of tumor-infiltrating lymphocytes and flow cytometric analysis of intracellular IFN-γ.

Statistics

Statistical analyses were performed using GraphPad Prism 8. Two-tailed unpaired Student's *t-test* was used for two-group comparisons, one-way ANOVA for multiple

groups, and Mann-Whitney U test for tumor burden data.

DATA AVAILABILITY

Data will be made available on request.

REFERENCES

1. Carding SR, Egan PJ. Gammadelta t cells: functional plasticity and heterogeneity (2002)
2. Vantourout P, Hayday A. Six-of-the-best: unique contributions of γδ t cells to immunology. *Nature Reviews. Immunology* **13**, 88-100 (2013). https://doi.org/10.1038/nri3384
3. Chien Y, Meyer C, Bonneville M. Γδ t cells: first line of defense and beyond. *Annu Rev Immunol* **32**, 121-55 (2014). https://doi.org/10.1146/annurev-immunol-032713-120216
4. Mckenzie DR, Kara EE, Bastow CR, Tyllis TS, Fenix KA, Gregor CE, Wilson JJ, Babb R, Paton JC, Kallies A, Nutt SL, Brüstle A, Mack M, Comerford I, Mccoll SR. Il-17-producing γδ t cells switch migratory patterns between resting and activated states. *Nat Commun* **8**, 15632 (2017). https://doi.org/10.1038/ncomms15632
5. Mensurado S, Blanco-Domínguez R, Silva-Santos B. The emerging roles of γδ t cells in cancer immunotherapy. *Nature Reviews. Clinical Oncology* **20**, 178-91 (2023). https://doi.org/10.1038/s41571-022-00722-1
6. Shiromizu CM, Jancic CC. Γδ t lymphocytes: an effector cell in autoimmunity and infection. *Front Immunol* **9**, 2389 (2018). https://doi.org/10.3389/fimmu.2018.02389
7. Arias-Badia M, Chang R, Fong L. Γδ t cells as critical anti-tumor immune effectors. *Nature Cancer* **5**, 1145-57 (2024). https://doi.org/10.1038/s43018-024-00798-x
8. Hayday A, Dechanet-Merville J, Rossjohn J, Silva-Santos B. Cancer immunotherapy by γδ t cells. *Science (New York, N.Y.)* **386**, eabq7248 (2024). https://doi.org/10.1126/science.abq7248
9. Xiong N, Raulet DH. Development and selection of gammadelta t cells. *Immunol Rev* **215**, 15-31 (2007). https://doi.org/10.1111/j.1600-065X.2006.00478.x
10. Silva-Santos B, Mensurado S, Coffelt SB. Γδ t cells: pleiotropic immune effectors with therapeutic potential in cancer. *Nature Reviews. Cancer* **19**, 392-404 (2019). https://doi.org/10.1038/s41568-019-0153-5
11. Papotto PH, Ribot JC, Silva-Santos B. Il-17(+) γδ t cells as kick-starters of inflammation. *Nat Immunol* **18**, 604-11 (2017). https://doi.org/10.1038/ni.3726
12. Hu X, Lin S, Meng W, Liu H, Qin Z, Wu Z, Wan Y, Ma S, Yang X, Yin Z, Chu Y, Zhang W, Shao L, Lin Y. Il-17a-producing γδ t cells control pulmonary mycobacterium abscessus infection in mice. *Nat Microbiol*, 10-1038 (2026). https://doi.org/10.1038/s41564-026-02466-5
13. Deretic V. Autophagy in inflammation, infection, and immunometabolism. *Immunity* **54**, 437-53 (2021). https://doi.org/10.1016/j.immuni.2021.01.018
14. Rodrigues PM, Sousa LG, Perrod C, Maceiras AR, Ferreirinha P, Pombinho R, Romera-Cárdenas G, Gomez-Lazaro M, Senkara M, Pistolic J, Cabanes D, Klein L, Saftig P, Alves NL. Lamp2 regulates autophagy in the thymic epithelium and thymic stroma-dependent cd4 t cell development. *Autophagy* **19**, 426-39 (2023). https://doi.org/10.1080/15548627.2022.2074105
15. Pua HH, Dzhagalov I, Chuck M, Mizushima N, He Y. A critical role for the autophagy gene atg5 in t cell survival and proliferation. *The Journal of Experimental Medicine* **204**, 25-31 (2007). https://doi.org/10.1084/jem.20061303

16. O'Sullivan TE, Geary CD, Weizman O, Geiger TL, Rapp M, Dorn GWN, Overholtzer M, Sun JC. Atg5 is essential for the development and survival of innate lymphocytes. *Cell Rep* **15**, 1910-9 (2016). https://doi.org/10.1016/j.celrep.2016.04.082
17. Ohashi Y. Activation mechanisms of the vps34 complexes. *Cells-Basel* **10**, 3124 (2021). https://doi.org/10.3390/cells10113124
18. Liu F, Wu X, Qian Y, Jiang X, Wang Y, Gao J. Pik3c3 regulates the expansion of liver cscs and pik3c3 inhibition counteracts liver cancer stem cell activity induced by pi3k inhibitor. *Cell Death Dis* **11**, 427 (2020). https://doi.org/10.1038/s41419-020-2631-9
19. Jiang X, Bao Y, Liu H, Kou X, Zhang Z, Sun F, Qian Z, Lin Z, Li X, Liu X, Jiang L, Yang Y. Vps34 stimulation of p62 phosphorylation for cancer progression. *Oncogene* **36**, 6850-62 (2017). https://doi.org/10.1038/onc.2017.295
20. Elkholi IE, Robert A, Malouf C, Wu JL, Kuasne H, Drapela S, Macleod G, Hébert S, Pacis A, Calderon V, Kleinman CL, Gomes AP, Alvarez JV, Aguirre-Ghiso JA, Park M, Angers S, C Té JO. Targeting the dependence on pik3c3-mtorc1 signaling in dormancy-prone breast cancer cells blunts metastasis initiation. *Cancer Res* **85**, 2179-98 (2025). https://doi.org/10.1158/0008-5472.CAN-23-2654
21. Mcleod IX, Zhou X, Li Q, Wang F, He Y. The class iii kinase vps34 promotes t lymphocyte survival through regulating il-7rα surface expression. *Journal of Immunology (Baltimore, Md. : 1950)* **187**, 5051-61 (2011). https://doi.org/10.4049/jimmunol.1100710
22. Feng P, Yang Q, Luo L, Guan Z, Fu J, Zhao M, Meng W, Wan S, He J, Li Z, Wang G, Sun G, Dong Z, Yang M. Vps34 sustains treg cell survival and function via regulating intracellular redox homeostasis. *Cell Death Differ* **31**, 1519-33 (2024). https://doi.org/10.1038/s41418-024-01353-y
23. Yang G, Song W, Xu J, Postoak JL, Cheng F, Martinez J, Zhang J, Wu L, Van Kaer L. Pik3c3 deficiency in myeloid cells imparts partial resistance to experimental autoimmune encephalomyelitis associated with reduced il-1β production. *Cell Mol Immunol* **18**, 2024-39 (2021). https://doi.org/10.1038/s41423-020-00589-1
24. Yang G, Postoak JL, Song W, Martinez J, Zhang J, Wu L, Van Kaer L. Dendritic cell pik3c3/vps34 controls the pathogenicity of cns autoimmunity independently of lc3-associated phagocytosis. *Autophagy* **18**, 161-70 (2022). https://doi.org/10.1080/15548627.2021.1922051
25. Wang S, Xia P, Huang G, Zhu P, Liu J, Ye B, Du Y, Fan Z. Foxo1-mediated autophagy is required for nk cell development and innate immunity. *Nat Commun* **7**, 11023 (2016). https://doi.org/10.1038/ncomms11023
26. Yang G, Song W, Postoak JL, Chen J, Martinez J, Zhang J, Wu L, Van Kaer L. Autophagy-related protein pik3c3/vps34 controls t cell metabolism and function. *Autophagy* **17**, 1193-204 (2021). https://doi.org/10.1080/15548627.2020.1752979
27. Coffey F, Lee S, Buus TB, Lauritsen JH, Wong GW, Joachims ML, Thompson LF, Zú Iga-Pflücker JC, Kappes DJ, Wiest DL. The tcr ligand-inducible expression of cd73 marks γδ lineage commitment and a metastable intermediate in effector specification. *The Journal of Experimental Medicine* **211**, 329-43 (2014). https://doi.org/10.1084/jem.20131540
28. Fahl SP, Contreras AV, Verma A, Qiu X, Harly C, Radtke F, Zú Iga-Pflücker JC, Murre C, Xue H, Sen JM, Wiest DL. The e protein-tcf1 axis controls γδ t?cell development and effector fate. *Cell Rep* **34**, 108716 (2021). https://doi.org/10.1016/j.celrep.2021.108716
29. Luo C, Li Y, Wang H, Feng Z, Li Y, Long J, Liu J. Mitochondrial accumulation under oxidative stress is due to defects in autophagy. *J Cell Biochem* **114**, 212-9 (2013). https://doi.org/10.1002/jcb.24356
30. Wang C, Zhang W, Shu Y, Song L, Wan Y, Zhang H, Bo L, Guo Y. Metabolic control of immunity

and inflammation: mitochondrial dynamics, pharmacological targets, and therapeutic opportunities. *Pharmacol Res* **227**, 108194 (2026). https://doi.org/10.1016/j.phrs.2026.108194
31. Argüello RJ, Combes AJ, Char R, Gigan J, Baaziz AI, Bousiquot E, Camosseto V, Samad B, Tsui J, Yan P, Boissonneau S, Figarella-Branger D, Gatti E, Tabouret E, Krummel MF, Pierre P. Scenith: a flow cytometry-based method to functionally profile energy metabolism with single-cell resolution. *Cell Metab* **32**, 1063-75 (2020). https://doi.org/10.1016/j.cmet.2020.11.007
32. Pietraforte D, Malorni W. Focusing at the double-edged sword of redox imbalance: signals for cell survival or for cell death? *Antioxid Redox Sign* **21**, 52-5 (2014). https://doi.org/10.1089/ars.2014.5914
33. Su L, Zhang J, Gomez H, Murugan R, Hong X, Xu D, Jiang F, Peng Z. Reactive oxygen species-induced lipid peroxidation in apoptosis, autophagy, and ferroptosis. *Oxid Med Cell Longev* **2019**, 5080843 (2019). https://doi.org/10.1155/2019/5080843
34. Ugur M, Kaminski A, Pabst O. Lymph node γδ and αβ cd8(+) t cells share migratory properties. *Sci Rep-Uk* **8**, 8986 (2018). https://doi.org/10.1038/s41598-018-27339-8
35. Cai Y, Shen X, Ding C, Qi C, Li K, Li X, Jala VR, Zhang H, Wang T, Zheng J, Yan J. Pivotal role of dermal il-17-producing γδ t cells in skin inflammation. *Immunity* **35**, 596-610 (2011). https://doi.org/10.1016/j.immuni.2011.08.001
36. Bharath LP, Nikolajczyk BS. The intersection of metformin and inflammation. *American Journal of Physiology. Cell Physiology* **320**, C873-9 (2021). https://doi.org/10.1152/ajpcell.00604.2020
37. Parekh VV, Wu L, Boyd KL, Williams JA, Gaddy JA, Olivares-Villagómez D, Cover TL, Zong W, Zhang J, Van Kaer L. Impaired autophagy, defective t cell homeostasis, and a wasting syndrome in mice with a t cell-specific deletion of vps34. *Journal of Immunology (Baltimore, Md. : 1950)* **190**, 5086-101 (2013). https://doi.org/10.4049/jimmunol.1202071
38. Norton EG, Chapman NM, Shi H, Meng X, Huang H, Kc A, Rankin S, Saravia J, Yuan S, Hu H, Vogel P, Chi H. Vps34-orchestrated lipid signaling processes regulate the transitional heterogeneity and functional adaptation of effector regulatory t cells. *Plos Biol* **23**, e3003074 (2025). https://doi.org/10.1371/journal.pbio.3003074
39. Willinger T, Flavell RA. Canonical autophagy dependent on the class iii phosphoinositide-3 kinase vps34 is required for naive t-cell homeostasis. *P Natl Acad Sci Usa* **109**, 8670-5 (2012). https://doi.org/10.1073/pnas.1205305109
40. Jensen KDC, Su X, Shin S, Li L, Youssef S, Yamasaki S, Steinman L, Saito T, Locksley RM, Davis MM, Baumgarth N, Chien Y. Thymic selection determines gammadelta t cell effector fate: antigen-naive cells make interleukin-17 and antigen-experienced cells make interferon gamma. *Immunity* **29**, 90-100 (2008). https://doi.org/10.1016/j.immuni.2008.04.022
41. Voss K, Sewell AE, Krystofiak ES, Gibson-Corley KN, Young AC, Basham JH, Sugiura A, Arner EN, Beavers WN, Kunkle DE, Dickson ME, Needle GA, Skaar EP, Rathmell WK, Ormseth MJ, Major AS, Rathmell JC. Elevated transferrin receptor impairs t cell metabolism and function in systemic lupus erythematosus. *Science Immunology* **8**, eabq0178 (2023). https://doi.org/10.1126/sciimmunol.abq0178
42. Qin X, Zhong H, Liu M, Yu T, Ma R, Zhou Y, Chen J, Liu F, Wang X, Long J. Metformin drives hif-1α-mediated dual metabolic reprogramming to enhance γδ t cell therapy in triple-negative breast cancer. *Cancer Immunology, Immunotherapy : Cii* **75**, 133 (2026). https://doi.org/10.1007/s00262-026-04351-w
43. Yang Z, Liu Y, Han Y, Tan L, Wang S, Zhang S, Li C, He P, Zhang Y, Ji Y, Yin Z, Li J, Ren F. Metformin sensitizes esophageal squamous cell carcinoma to vγ9vδ2 t cell-mediated cytotoxicity by upregulating btn3a1 and btn2a1. *Cell Death Dis* **17**, 708 (2026). https://doi.org/10.1038/s41419-

026-08924-6
44. Argüello RJ, Combes AJ, Char R, Gigan JP, Baaziz AI, Bousiquot E, Camosseto V, Samad B, Tsui J, Yan P, Boissonneau S, Figarella-Branger D, Gatti E, Tabouret E, Krummel MF, Pierre P. Scenith: a flow cytometry-based method to functionally profile energy metabolism with single-cell resolution. *Cell Metab* **32**, 1063-75 (2020). https://doi.org/10.1016/j.cmet.2020.11.007

AUTHOR CONTRIBUTIONS

JF, PF, ZG and BX contributed equally to this work. JF, PF, ZG and BX performed the experiments, acquired, analyzed and interpreted data, prepared figures, and drafted the manuscript; JH, BG and HS provided technical support and assisted with animal experiments and sample preparations; BG, HS, JY and MY obtained funding; JY and MY conceived and designed the study, supervised the research, critically revised the manuscript, and administered the project. All authors read and approved the final manuscript.

ACKNOWLEDGMENT

This work was supported by the Natural Science Foundation of China (82571993, 82271754, 82301974); Natural Science Foundation of Guangdong Province (2024A1515010566, 2026A1515012455); Guangdong Basic and Applied Basic Research Foundation (2025A1515140169); the Joint Funds of Yunnan Province and Kunming Medical University (202301AY070001-003, 202401AY070001-301); the High-Level Talent Project of Yunnan Province (YNQR-QNRC-2018-126, D-2024048); and Guangzhou Key Laboratory for Germ-free animals and Microbiota Application (202201020381).

COMPETING INTERESTS

The authors declare that they have no conflict of interest.

FIGURE LEGENDS

Figure 1. Autophagic flux dynamics during thymocyte development and in γδ T cells. (A) Representative flow plots of RFP and EGFP signals in thymocyte subsets (DN, DP, $CD4^+$, $CD8^+$) from *CAG-RFP-EGFP-LC3* transgenic mice. (B) Quantification of

EGFP$^+$RFP$^+$ (autophagosome-containing, left) and EGFP$^-$RFP$^+$ (autolysosome-containing, right) cell percentages in the indicated thymocyte subsets (n = 4). (C, D) Representative histograms (left) and quantification (right) of LC3B (C) and autophagosome (D) MFI in thymocyte subsets from wild-type (WT) mice (n = 3). (E) Representative flow plots of RFP and EGFP signals in thymocyte subsets from *CAG-RFP-EGFP-LC3* mice treated with DMSO (top) or bafilomycin A1 (BafA1, bottom). (F) Quantification of EGFP$^+$RFP$^+$ cell percentages in thymocyte subsets with DMSO or BafA1 treatment (n = 4). (G) Representative flow plots of RFP and EGFP signals in thymic γδ T and αβ T cells from *CAG-RFP-EGFP-LC3* transgenic mice. (H) Quantification of EGFP$^+$RFP$^+$ (left) and EGFP$^-$RFP$^+$ (right) cell percentages in thymic γδ T and αβ T cells (n = 4). (I, J) Representative histograms (left) and quantification of LC3B (I) and autophagosome (J) MFI (right) in thymic γδ T and αβ T cells from WT mice (n = 3). (K, L) Representative flow plots (left) and quantification (right) of EGFP$^+$RFP$^+$ cell percentages in BafA1/DMSO-treated thymic (K) and splenic (L) γδ T cells from *CAG-RFP-EGFP-LC3* mice (n = 4). Data are presented as mean ± SD and represent three independent experiments. *P < 0.05, **P < 0.01, ***P < 0.001.

Figure 2. VPS34 deficiency blocks autophagic flux in γδ T cells. (A-C) Representative histograms (left) and corresponding quantification (right) for LC3B (A), p62 (B), and autophagosome signal (C) in CD3$^+$TCRγδ$^+$ cells from *Pik3c3$^{fl/fl}$* and *Pik3c3$^{fl/fl}$CD2^{Cre}* mice (n = 4). (D, E) Western blot analysis of LC3 II and p62 protein levels in WT γδ T cells treated with DMSO (vehicle) or VPS34-IN-1 (5 μM, 24 h), with BafA1 (100 nM, 4 h) added during the final 4 h of incubation. GAPDH was used as the loading control (n = 4). (F, G) Representative flow plots and quantification of EGFP$^+$RFP$^+$ and EGFP$^-$RFP$^+$ populations in γδ T cells from *CAG-RFP-EGFP-LC3* mice treated with DMSO (vehicle) or VPS34-IN-1 (5 μM 24 h), with BafA1 (100 nM, 4 h) added during the final 4 h of incubation (n = 4). Data are presented as mean ± SD and are representative of three independent experiments. *P < 0.05, **P < 0.01, ***P < 0.001.

Figure 3. Deletion of VPS34 disrupts thymocyte development and peripheral T cell homeostasis. (A) Representative macroscopic images of thymi isolated from *Pik3c3$^{fl/fl}$* and *Pik3c3$^{fl/fl}$CD2^{Cre}* (cKO) mice. (B) Quantification of thymus weight (left) and total thymic lymphocyte counts (right) from WT and cKO mice (n = 4). (C) Representative

flow plots (left) and quantitative analysis (right) of CD4/CD8-defined thymocyte subsets (DN, DP, $CD4^+$, $CD8^+$) from WT and cKO mice (n = 4). (D) Representative flow plots (left) and quantification (right) of CD44/CD25-defined DN thymocyte subsets (DN1-DN4) from WT and cKO mice (n = 4). (E) Representative histograms (left) and MFI quantification (right) of CD25 expression in DN thymocytes from WT and cKO mice (n = 4). (F) Representative flow plots (left) and absolute cell counts (right) of γδ T cells in the thymus from *Pik3c3*$^{fl/fl}$ and *Pik3c3*$^{fl/fl}$*CD2*^{Cre} mice (n = 4). (G) Representative flow plots (left) and quantitative analysis (right) of γδ T cell maturation subsets (uncom.: $CD24^+CD73^-$, com.: $CD24^+CD73^+$, mature: $CD24^-CD73^+$) in the thymus from WT and cKO mice (n = 4). (H) Representative flow plots (left) and quantitative analysis (right) of $V\gamma1^+$, $V\gamma4^+$ and $V\gamma1^-V\gamma4^-$ cells in thymic γδ T cells from *Pik3c3*$^{fl/fl}$ and *Pik3c3*$^{fl/fl}$*CD2*^{Cre} mice (n = 4). (I-K) Representative flow plots (left) and quantitative analysis (right) of $V\gamma4^+$ (I), $V\gamma1^+$ (J) and $V\gamma1^-V\gamma4^-$ (K) T cell maturation subsets in the thymus from WT and cKO mice (n = 4). All data are presented as mean ± SD and represent three independent experiments. **P* < 0.05, ***P* < 0.01, ****P* < 0.001.

Figure 4. Loss of VPS34 disrupts peripheral γδ T cell maintenance and subset homeostasis. (A) Representative flow plots (left) and absolute cell counts (right) of γδ T cells in the spleen and LNs from *Pik3c3*$^{fl/fl}$ and *Pik3c3*$^{fl/fl}$*CD2*^{Cre} mice (n = 4). (B, C) Representative flow plots (B) and quantification (C) of γδ T cell subsets (Vγ4, Vγ1, $V\gamma4^-V\gamma1^-$) in the spleen and LNs from *Pik3c3*$^{fl/fl}$ and *Pik3c3*$^{fl/fl}$*CD2*^{Cre} mice (n = 4). (D) Schematic of the competitive bone marrow chimera experimental setup. (E) Representative flow plots (left) and quantitative analysis (right) for WT ($CD45.1^+$) and cKO ($CD45.2^+$) γδ T cell frequencies among total γδ T cells in the spleen and LNs from recipient chimeric mice (n = 3). (F, G) Representative flow plots (F) and absolute cell counts (G) of γδ T cells in multiple peripheral tissues, including skin, colonic lamina propria (cLP), small intestine (SI), liver and lung from WT and cKO mice (n = 7). (H) Representative flow plots of skin γδ T cell subsets (epidermis and dermis) from WT and cKO mice. (I) Quantification of the percentage (left) and absolute cell counts (right) of epidermal and dermal γδ T cells from WT and cKO mice (n = 7). All data are presented as mean ± SD and represent at least three independent experiments. **P* < 0.05, ***P* < 0.01, ****P* < 0.001.

Figure 5. VPS34 deficiency induces mitochondrial dysfunction and oxidative stress in γδ T cells. (A, B) Representative histograms (left) and quantification (right) of mitochondrial mass (mitoTracker MFI) (A) and mitochondrial membrane potential (TMRM MFI) (B) in γδ T cells from *Pik3c3*$^{fl/fl}$ (WT) and *Pik3c3*$^{fl/fl}$*CD2*^{Cre} (cKO) mice (n = 4). (C) Metabolic capacity profiling of WT and cKO γδ T cells (n = 3). (D) Representative flow plots (left) and quantification (right) of Ki67^{+} proliferating γδ T cells from WT and cKO mice (n = 4). (E) Quantification of forward scatter (FSC-A) and side scatter (SSC-A) as indicators of cell size and granularity for WT and cKO γδ T cells (n = 4). (F, G) Representative histograms (left) and quantification (right) of cellular ROS (CellROX MFI) (F) and mitochondrial superoxide (mitoSOX MFI) (G) in WT and cKO γδ T cells (n = 4). (H) Representative histograms (left) and quantification (right) of 7-AAD^{+} dead γδ T cells from WT and cKO mice (n = 4). (I) Representative histograms (left) and quantification (right) of cellular ROS (CellROX MFI) in WT and cKO γδ T cells treated with DMSO (vehicle) or N-acetylcysteine (NAC, 5 mM, 24 h) (n = 3). (J) Representative flow plots (left) and quantification (right) of 7-AAD^{+} dead γδ T cells from WT and cKO mice treated with DMSO or NAC (5 mM, 24 h) (n = 3). All data are presented as mean ± SD and represent at least three independent experiments. *$P < 0.05$, **$P < 0.01$, ***$P < 0.001$.

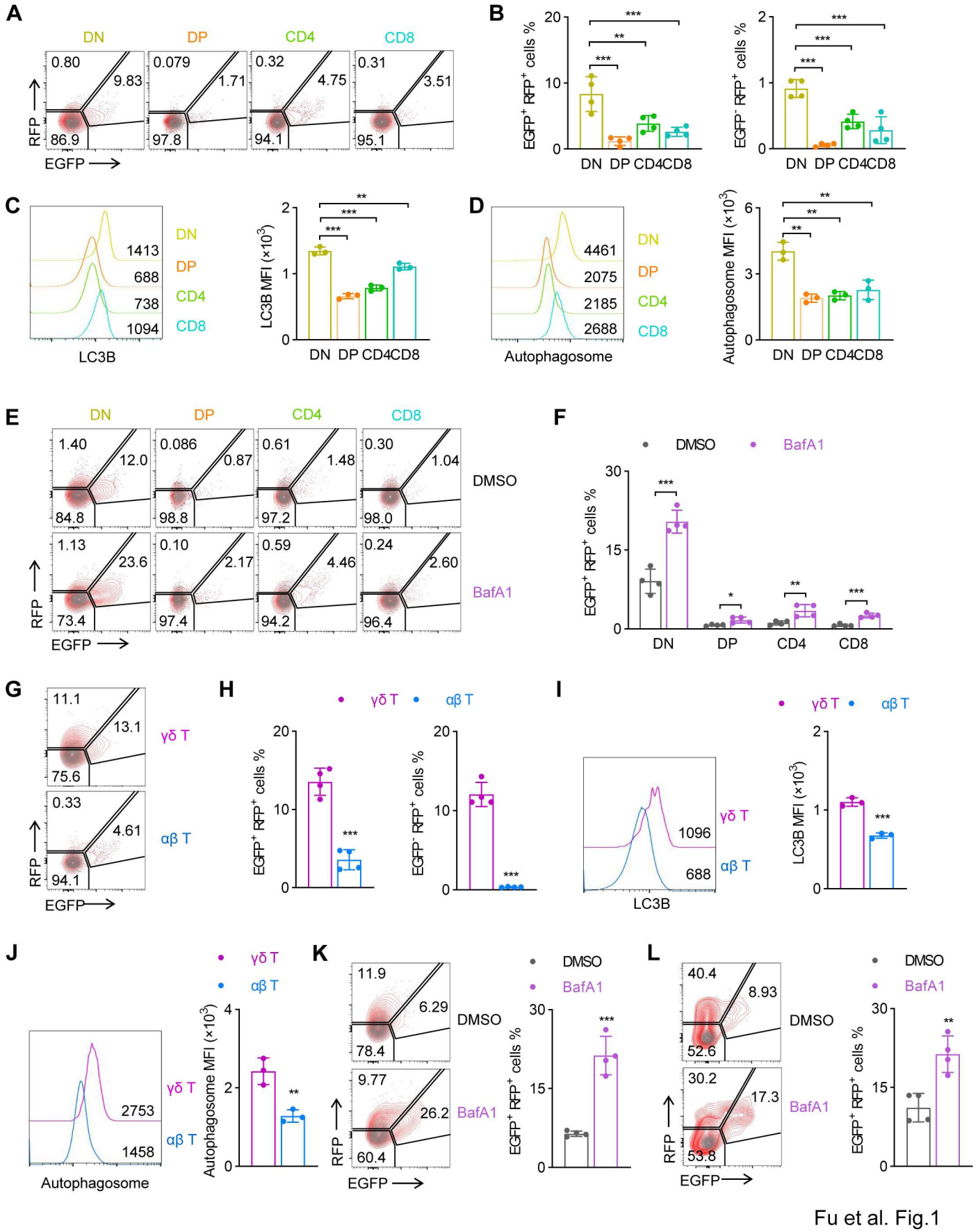
Figure 6. VPS34 deficiency promotes lipid accumulation and ferroptosis in γδ T cells. (A-D) Representative histograms (left) and quantification (right) of iron levels (FerroOrange MFI) (A), CD71 (transferrin receptor) (B), CD36 (fatty acid translocase) expression (C), and intracellular lipid accumulation (Bodipy C11 MFI) (D) in γδ T cells from *Pik3c3*$^{fl/fl}$ (WT) and *Pik3c3*$^{fl/fl}$*CD2*^{Cre} (cKO) mice (n = 4). (E) Representative flow plots (left) and quantification (right) of 7-AAD^{+} dead γδ T cells in WT and cKO mice treated with DMSO (vehicle) or Ferrostatin-1 (Fer-1, 10 μM, 24 h) (n = 3). (F) Representative flow plots (left) and quantification (right) of Annexin V^{+} apoptotic γδ T cells from WT and cKO mice (n = 4). (G, H) Representative histograms (left) and quantification (right) of cleaved Caspase-3 (G) and Bim (H) expression (MFI) in WT and cKO γδ T cells (n = 4). (I) Representative flow cytometry plots (left) and quantification (right) of 7-AAD^{+} dead γδ T cells in WT and cKO mice treated with DMSO, Z-VAD-FMK (Z-V-F, 20 μM, 24 h, apoptosis inhibitor), or a combination of Fer-1 and Z-V-F

(Combo) for 24 h (n = 3). All data are presented as mean ± SD and represent at least three independent experiments. $^{**}P < 0.01$, $^{***}P < 0.001$.

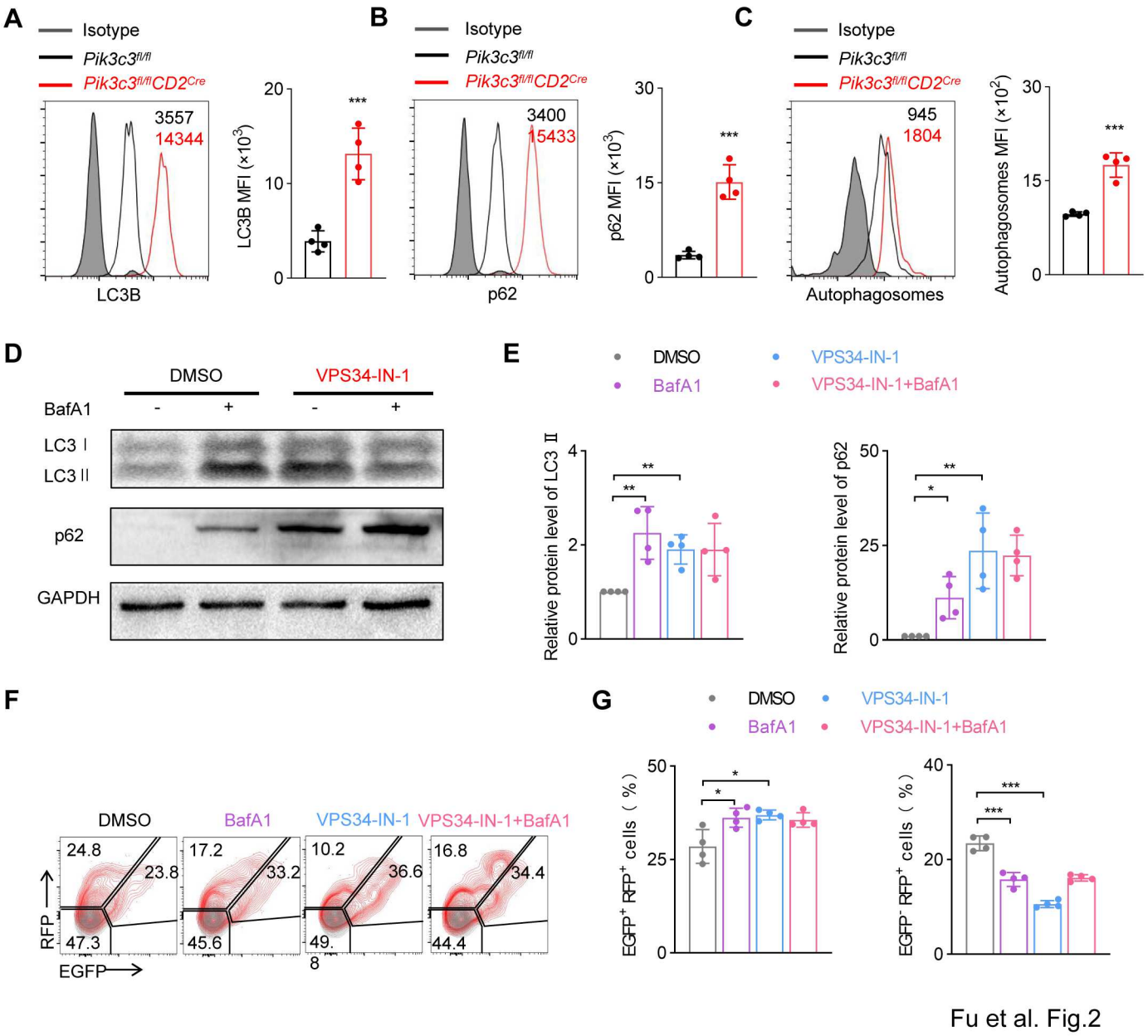
Figure 7. VPS34 deficiency disrupts CD44^{hi} effector γδ T cell homeostasis via mitochondrial dysfunction and cell death. (A, B) Representative flow plots (left) and percentages (right) of CD44^{-}CD62L^{+} naïve and CD44^{+}CD62L^{-} effector γδ T cell subsets in the spleen (A) and LNs (B) from *Pik3c3$^{fl/fl}$* (WT) and *Pik3c3$^{fl/fl}$CD2^{Cre}* (cKO) mice (n = 4). (C, D) Representative flow plots (C) and quantification (D) of Annexin V^{+} and 7-AAD^{+} cells in CD44^{hi} and CD44^{lo} γδ T cell subsets from WT and cKO mice (n = 4). (E-I) Representative histograms (left) and quantification (right) of mitochondrial mass (mitoTracker MFI) (E), mitochondrial membrane potential (TMRM MFI) (F), total cellular ROS (CellROX MFI) (G), mitochondrial superoxide (mitoSOX MFI) (H), and intracellular lipid peroxidation (Bodipy C11 MFI) (I) in CD44^{hi} effector γδ T cells from WT and cKO mice (n = 4). All data are presented as mean ± SD and represent at least three independent experiments. $^{*}P < 0.05$, $^{**}P < 0.01$, $^{***}P < 0.001$.

Figure 8. VPS34 is essential for the functional maintenance and anti-tumor activity of γδ T cells. (A) Representative flow plots (left) and quantification (right) of IL-17^{+} γδ T cells in lymph nodes (LNs) from IMQ-treated *Pik3c3$^{fl/fl}$* (WT) and *Pik3c3$^{fl/fl}$CD2^{Cre}* (cKO) mice (n = 4). (B) Representative flow plots (left) and quantification (right) of IFN-γ^{+} and IL-17^{+} tumor-infiltrating γδ T cells from WT and cKO mice (n = 4). (C, D) Representative flow plots (left) and quantification (right) of IFN-γ^{+} (C) and IL-17^{+} (D) γδ T cells with or without VPS34-IN-1 treatment under γδ T1- and γδ T17-skewing conditions (n = 4). (E-G) Ex vivo expanded γδ T cells (treated with DMSO or VPS34-IN-1) were co-cultured with B16F0 melanoma cells and adoptively transferred into *TCRδ$^{-/-}$* mice. (E) Tumor growth kinetics curve; (F) representative tumor images; (G) quantification of final tumor weight (n = 5). (H) Quantification of LC3B MFI in γδ T cells with or without metformin treatment (n = 3). (I) Representative flow plots (left) and quantification (right) of IFN-γ^{+} γδ T cells with or without metformin treatment (n = 3). (J, K) Representative flow plots of 7-AAD^{+} dead B16F0 melanoma cells (J) and statistical analysis of γδ T cell-mediated specific killing (K) at different effector-to-target ratios, with or without metformin treatment (n = 3). (L) Schematic diagram of the in vivo adoptive transfer experiment in *Rag2$^{-/-}$* mice bearing B16F0 tumors. (M-O) Tumor growth

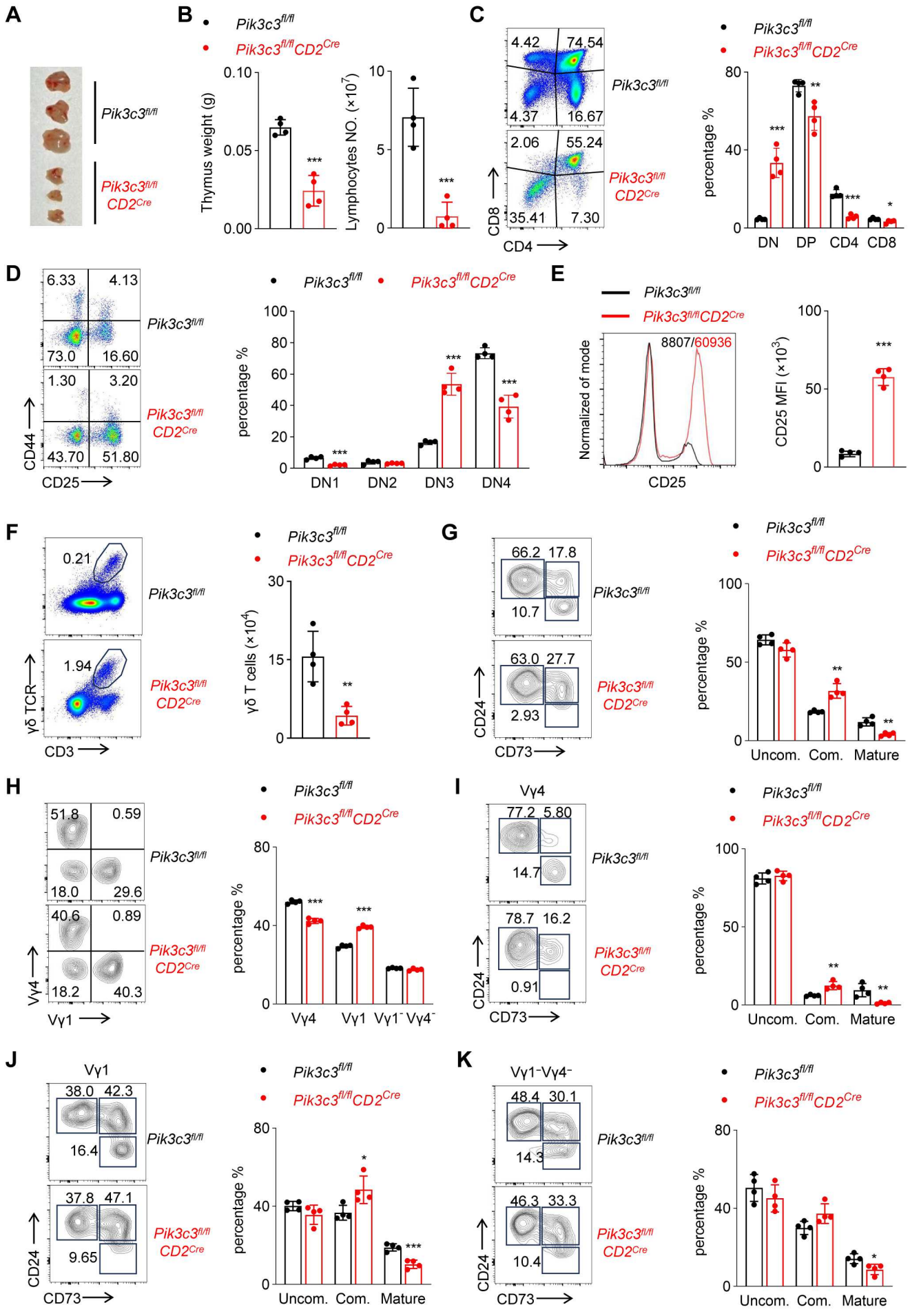
kinetics (M), representative tumor images (N), and quantification of final tumor weight (O) in mice receiving adoptively transferred γδ T cells with or without metformin (n = 5). (P) Quantification of IFN-γ^+ γδ T cells isolated from the adoptive transfer groups (n = 5). All data are presented as mean ± SD and represent at least three independent experiments, except for Fig. 8E and 8M, which are presented as mean ± SEM. *$P < 0.05$, **$P < 0.01$, ***$P < 0.001$.


A
DN
DP
CD4
CD8
0.80
9.83
86.9
0.079
1.71
97.8
0.32
4.75
94.1
0.31
3.51
95.1
RFP
EGFP
B
EGFP+ RFP+ cells %
EGFP- RFP+ cells %
DN DP CD4CD8
C
1413
688
738
1094
LC3B
LC3B MFI (×10^3)
D
4461
2075
2185
2688
Autophagosome
Autophagosome MFI (×10^3)
E
1.40
12.0
84.8
0.086
0.87
98.8
0.61
1.48
97.2
0.30
1.04
98.0
DMSO
1.13
23.6
73.4
0.10
2.17
97.4
0.59
4.46
94.2
0.24
2.60
96.4
BafA1
F
DMSO
BafA1
G
11.1
13.1
75.6
γδ T
0.33
4.61
94.1
αβ T
H
γδ T
αβ T
I
1096
688
LC3B
J
2753
1458
Autophagosome
Autophagosome MFI (×10^3)
K
11.9
6.29
78.4
9.77
26.2
60.4
L
40.4
8.93
52.6
30.2
17.3
53.8

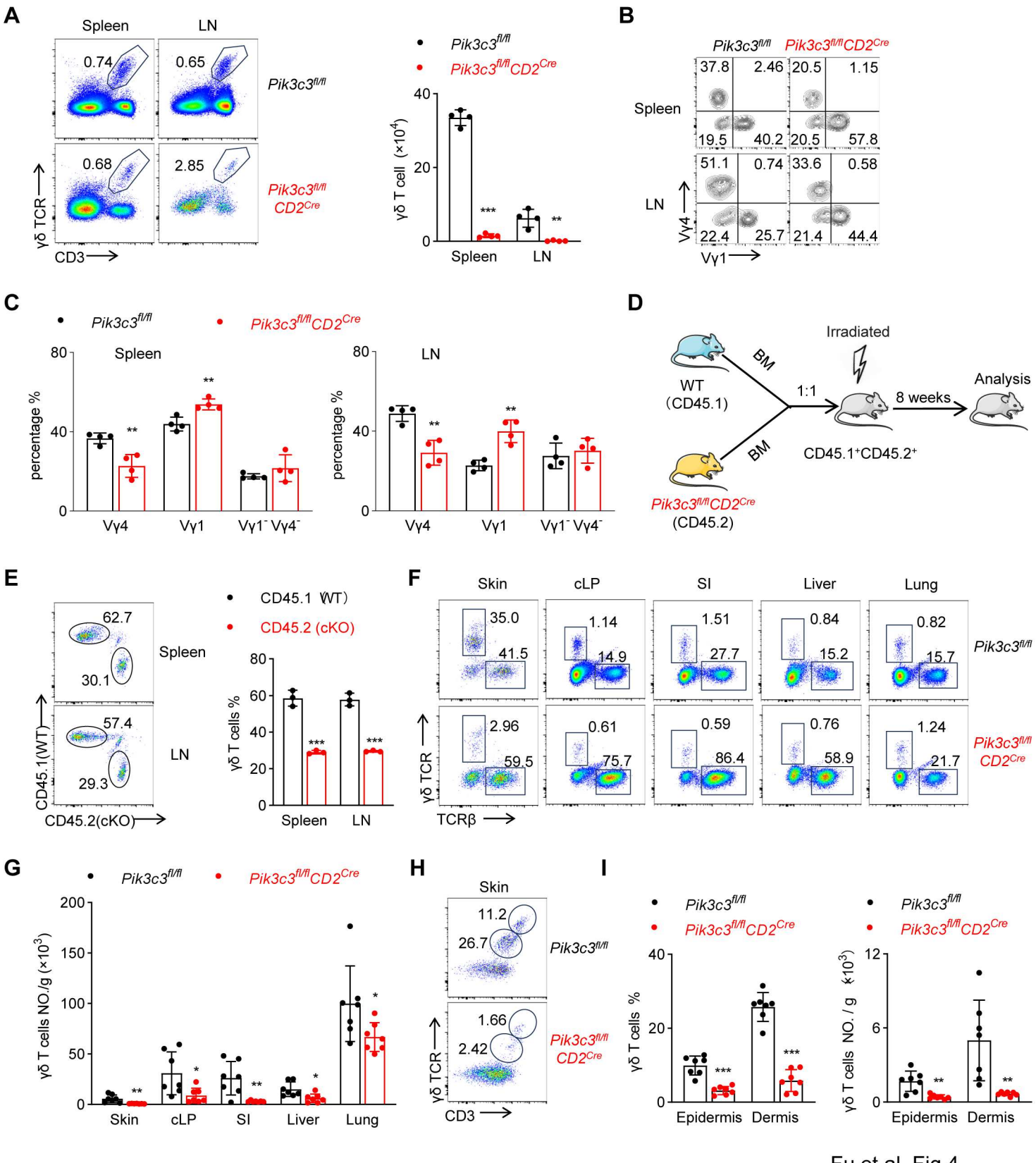
Fu et al. Fig.1


A
Isotype
Pik3c3fl/fl
Pik3c3fl/flCD2Cre
3557
14344
LC3B
LC3B MFI (×10^3)
***
B
Isotype
Pik3c3fl/fl
Pik3c3fl/flCD2Cre
3400
15433
p62
p62 MFI (×10^3)
***
C
Isotype
Pik3c3fl/fl
Pik3c3fl/flCD2Cre
945
1804
Autophagosomes
Autophagosomes MFI (×10^2)
***
D
DMSO
VPS34-IN-1
BafA1
LC3 I
LC3 II
p62
GAPDH
E
DMSO
VPS34-IN-1
BafA1
VPS34-IN-1+BafA1
Relative protein level of LC3 II
Relative protein level of p62
F
DMSO
BafA1
VPS34-IN-1
VPS34-IN-1+BafA1
24.8
23.8
47.3
17.2
33.2
45.6
10.2
36.6
49.8
16.8
34.4
44.4
RFP
EGFP
G
DMSO
VPS34-IN-1
BafA1
VPS34-IN-1+BafA1
EGFP+ RFP+ cells (%)
EGFP- RFP+ cells (%)

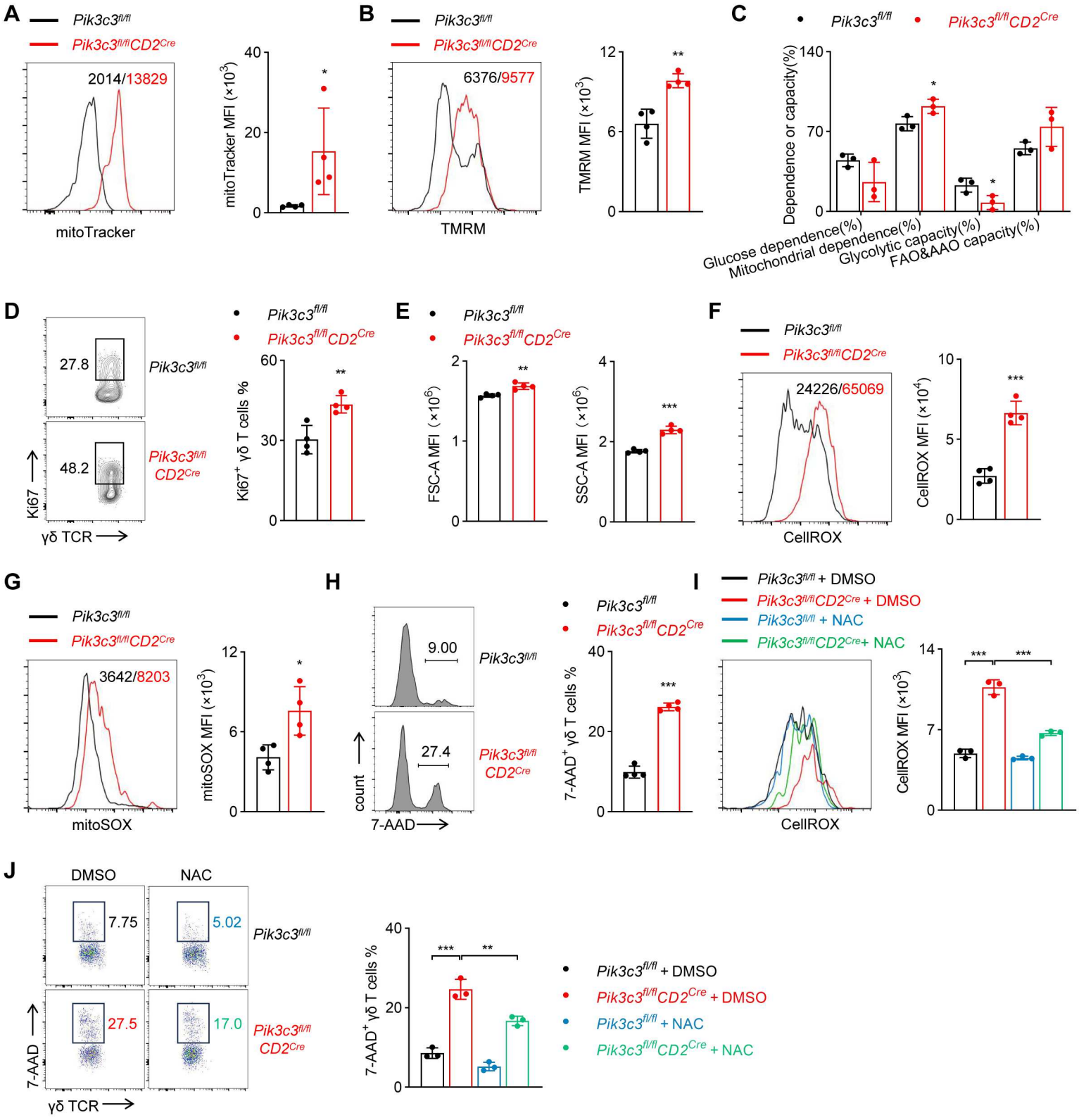
Fu et al. Fig.2


A
Pik3c3fl/fl
Pik3c3fl/fl CD2Cre
B
Pik3c3fl/fl
Pik3c3fl/fl CD2Cre
Thymus weight (g)
Lymphocytes NO. (×10^7)
C
4.42 74.54 4.37 16.67
2.06 55.24 35.41 7.30
CD8
CD4
percentage %
DN DP CD4 CD8
D
6.33 4.13 73.0 16.60
1.30 3.20 43.70 51.80
CD44
CD25
percentage %
DN1 DN2 DN3 DN4
E
Normalized of mode
8807/60936
CD25
CD25 MFI (×10^3)
F
0.21
1.94
γδ TCR
CD3
γδ T cells (×10^4)
G
66.2 17.8 10.7
63.0 27.7 2.93
CD24
CD73
percentage %
Uncom. Com. Mature
H
51.8 0.59 18.0 29.6
40.6 0.89 18.2 40.3
Vγ4
Vγ1
percentage %
Vγ4 Vγ1 Vγ1- Vγ4-
I
Vγ4
77.2 5.80 14.7
78.7 16.2 0.91
CD24
CD73
percentage %
Uncom. Com. Mature
J
Vγ1
38.0 42.3 16.4
37.8 47.1 9.65
CD24
CD73
percentage %
Uncom. Com. Mature
K
Vγ1-Vγ4-
48.4 30.1 14.3
46.3 33.3 10.4
CD24
CD73
percentage %
Uncom. Com. Mature

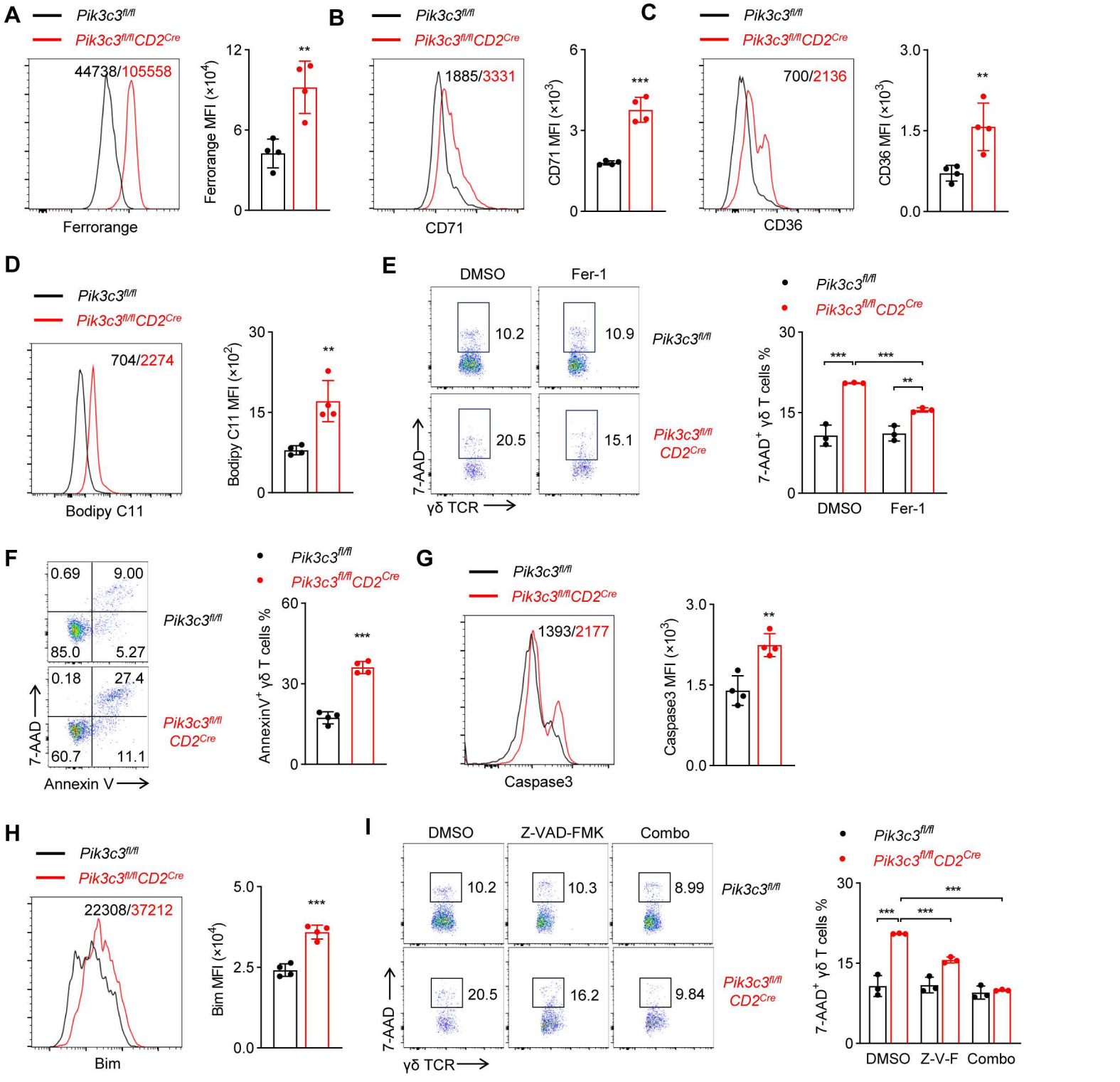
Fu et al. Fig.3


A
Spleen
LN
0.74
0.65
0.68
2.85
Pik3c3fl/fl
Pik3c3fl/fl CD2Cre
γδ TCR
CD3
Pik3c3fl/fl
Pik3c3fl/fl CD2Cre
γδ T cell (×10^4)
40
20
0
***
**
Spleen
LN
B
Pik3c3fl/fl
Pik3c3fl/fl CD2Cre
Spleen
LN
37.8
2.46
19.5
40.2
20.5
1.15
20.5
57.8
51.1
0.74
22.4
25.7
33.6
0.58
21.4
44.4
Vγ4
Vγ1
C
Pik3c3fl/fl
Pik3c3fl/fl CD2Cre
Spleen
LN
percentage %
80
40
0
**
Vγ4
Vγ1
Vγ1- Vγ4-
D
Irradiated
BM
BM
WT
(CD45.1)
1:1
8 weeks
Analysis
CD45.1+CD45.2+
Pik3c3fl/fl CD2Cre
(CD45.2)
E
62.7
30.1
57.4
29.3
Spleen
LN
CD45.1(WT)
CD45.2(cKO)
CD45.1 (WT)
CD45.2 (cKO)
γδ T cells %
80
60
40
20
0
***
Spleen
LN
F
Skin
cLP
SI
Liver
Lung
35.0
41.5
1.14
14.9
1.51
27.7
0.84
15.2
0.82
15.7
2.96
59.5
0.61
75.7
0.59
86.4
0.76
58.9
1.24
21.7
Pik3c3fl/fl
Pik3c3fl/fl CD2Cre
γδ TCR
TCRβ
G
Pik3c3fl/fl
Pik3c3fl/fl CD2Cre
γδ T cells NO./g (×10^3)
200
150
100
50
0
**
*
Skin
cLP
SI
Liver
Lung
H
Skin
11.2
26.7
1.66
2.42
Pik3c3fl/fl
Pik3c3fl/fl CD2Cre
γδ TCR
CD3
I
Pik3c3fl/fl
Pik3c3fl/fl CD2Cre
γδ T cells %
40
20
0
***
Epidermis
Dermis
γδ T cells NO. / g (×10^3)
12
6
0
**
Epidermis
Dermis

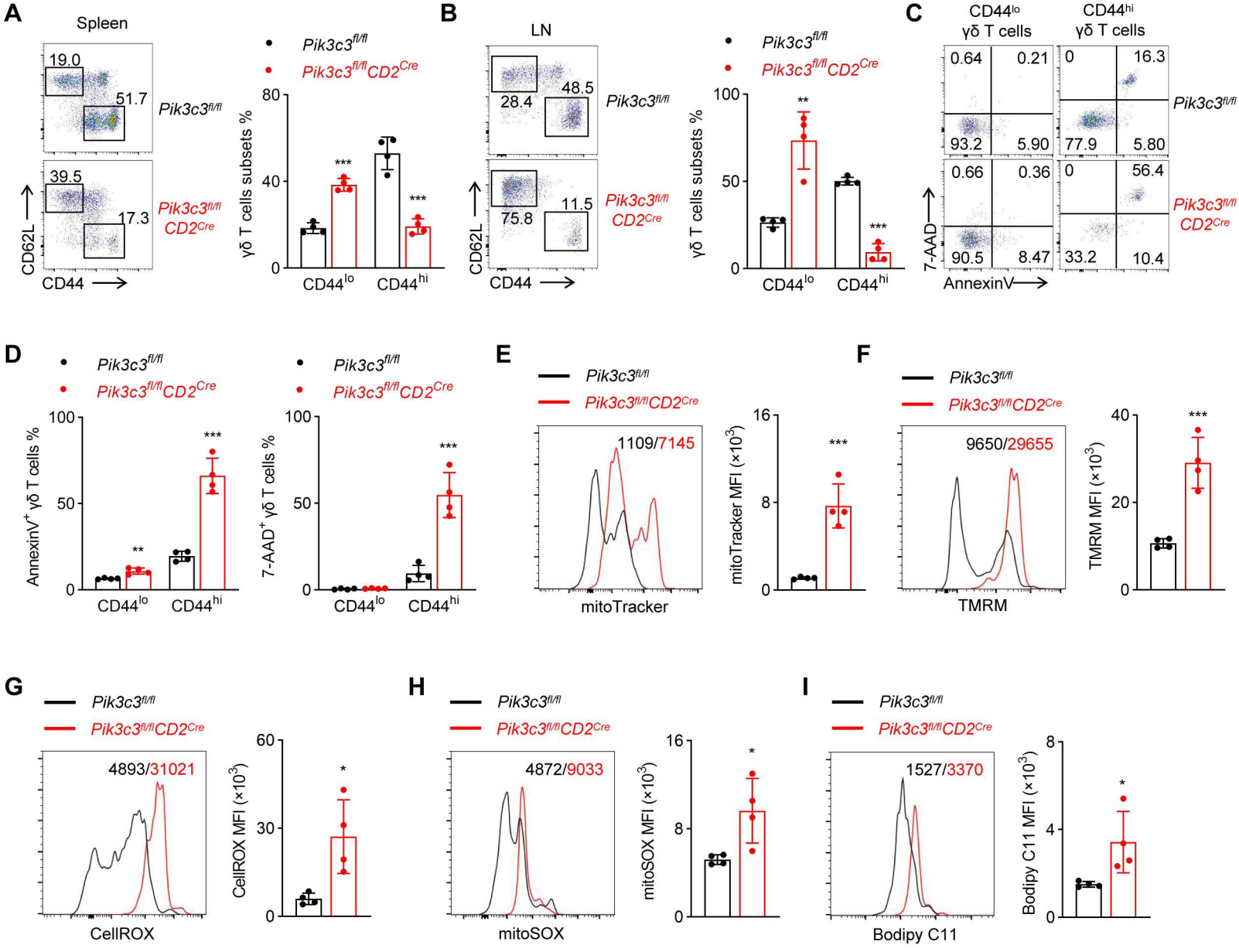
Fu et al. Fig.4


A
Pik3c3fl/fl
Pik3c3fl/flCD2Cre
2014/13829
mitoTracker
mitoTracker MFI (×10³)
B
6376/9577
TMRM
TMRM MFI (×10³)
C
Dependence or capacity(%)
Glucose dependence(%)
Mitochondrial dependence(%)
Glycolytic capacity(%)
FAO&AAO capacity(%)
D
27.8
48.2
Ki67
γδ TCR
Ki67⁺ γδ T cells %
E
FSC-A MFI (×10⁶)
SSC-A MFI (×10⁶)
F
24226/65069
CellROX
CellROX MFI (×10⁴)
G
3642/8203
mitoSOX
mitoSOX MFI (×10³)
H
9.00
27.4
count
7-AAD
7-AAD⁺ γδ T cells %
I
Pik3c3fl/fl + DMSO
Pik3c3fl/flCD2Cre + DMSO
Pik3c3fl/fl + NAC
Pik3c3fl/flCD2Cre+ NAC
CellROX
CellROX MFI (×10³)
J
DMSO
NAC
7.75
5.02
27.5
17.0
7-AAD
γδ TCR
7-AAD⁺ γδ T cells %

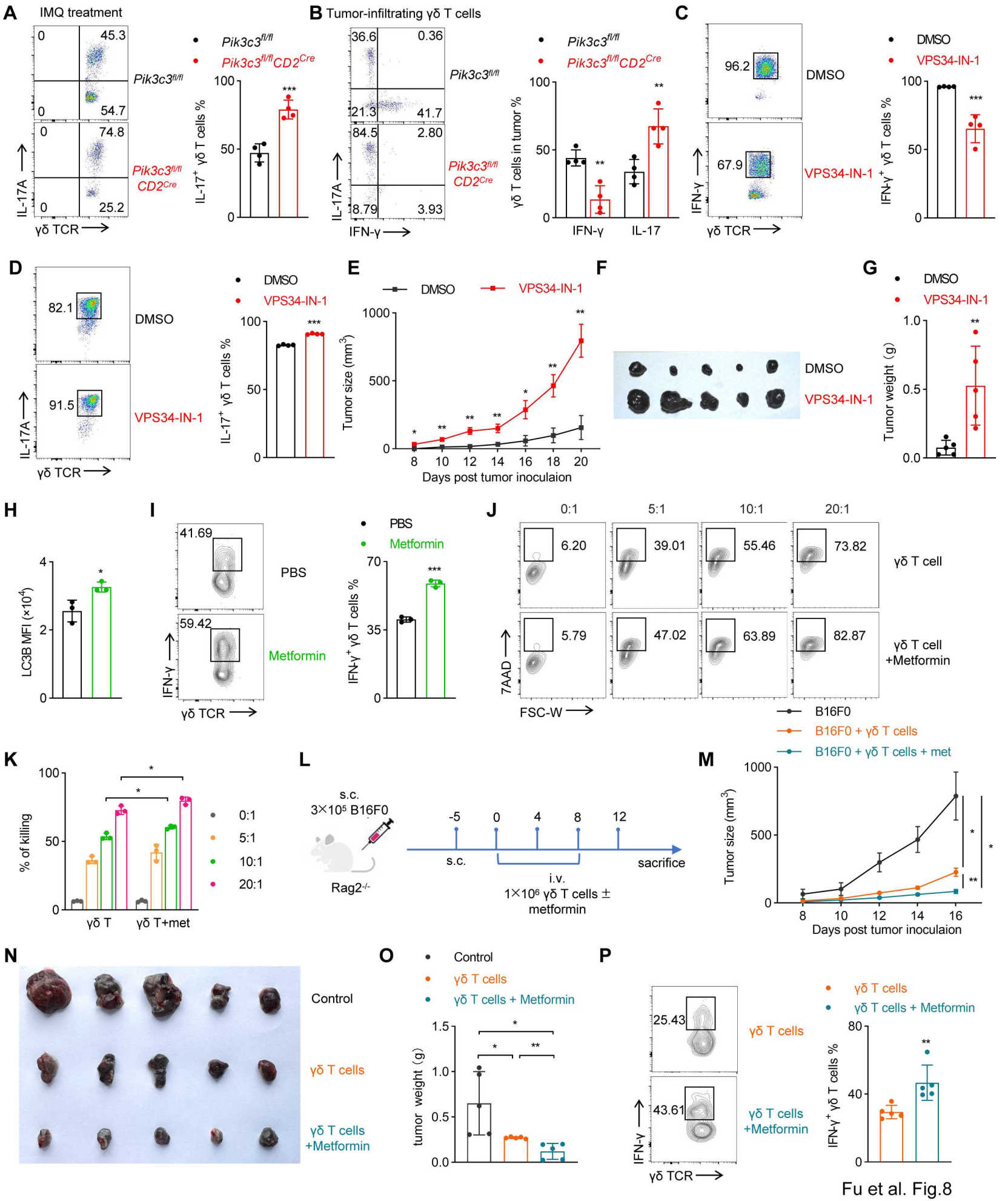
Fu et al. Fig.5


A
Pik3c3fl/fl
Pik3c3fl/flCD2Cre
44738/105558
Ferrorange
Ferrorange MFI (×10^4)
B
1885/3331
CD71
CD71 MFI (×10^3)
C
700/2136
CD36
CD36 MFI (×10^3)
D
704/2274
Bodipy C11
Bodipy C11 MFI (×10^2)
E
DMSO
Fer-1
10.2
10.9
20.5
15.1
7-AAD
γδ TCR
7-AAD+ γδ T cells %
F
0.69
9.00
85.0
5.27
0.18
27.4
60.7
11.1
Annexin V
AnnexinV+ γδ T cells %
G
1393/2177
Caspase3
Caspase3 MFI (×10^3)
H
22308/37212
Bim
Bim MFI (×10^4)
I
Z-VAD-FMK
Combo
10.3
8.99
16.2
9.84
DMSO
Z-V-F

Fu et al. Fig.6


A
Spleen
19.0
51.7
Pik3c3fl/fl
39.5
17.3
Pik3c3fl/fl CD2Cre
CD62L
CD44
Pik3c3fl/fl
Pik3c3fl/fl CD2Cre
γδ T cells subsets %
CD44lo
CD44hi
B
LN
48.5
28.4
11.5
75.8
C
CD44lo γδ T cells
CD44hi γδ T cells
0.64
0.21
93.2
5.90
0
16.3
77.9
5.80
0.66
0.36
90.5
8.47
0
56.4
33.2
10.4
7-AAD
AnnexinV
D
AnnexinV+ γδ T cells %
7-AAD+ γδ T cells %
E
1109/7145
mitoTracker
mitoTracker MFI (×10³)
F
9650/29655
TMRM
TMRM MFI (×10³)
G
4893/31021
CellROX
CellROX MFI (×10³)
H
4872/9033
mitoSOX
mitoSOX MFI (×10³)
I
1527/3370
Bodipy C11
Bodipy C11 MFI (×10³)

Fu et al. Fig.7


A
IMQ treatment
45.3
54.7
74.8
25.2
Pik3c3fl/fl
Pik3c3fl/fl CD2Cre
IL-17A
γδ TCR
IL-17+ γδ T cells %
B Tumor-infiltrating γδ T cells
36.6
0.36
21.3
41.7
84.5
2.80
18.79
3.93
IFN-γ
γδ T cells in tumor %
IL-17
C
96.2
67.9
DMSO
VPS34-IN-1
IFN-γ
IFN-γ+ γδ T cells %
D
82.1
91.5
E
Tumor size (mm3)
Days post tumor inoculaion
F
G
Tumor weight (g)
H
LC3B MFI (×10⁴)
I
41.69
59.42
PBS
Metformin
IFN-γ+ γδ T cells %
J
0:1
5:1
10:1
20:1
6.20
39.01
55.46
73.82
5.79
47.02
63.89
82.87
γδ T cell
γδ T cell +Metformin
7AAD
FSC-W
B16F0
B16F0 + γδ T cells
B16F0 + γδ T cells + met
K
% of killing
γδ T
γδ T+met
L
s.c.
3×10⁵ B16F0
Rag2-/-
-5
0
4
8
12
s.c.
i.v.
1×10⁶ γδ T cells ± metformin
sacrifice
M
N
Control
γδ T cells
γδ T cells +Metformin
O
tumor weight (g)
P
25.43
43.61

Fu et al. Fig.8

Supplementary Files

This is a list of supplementary files associated with this preprint. Click to download.

- Supplementaryinformation.docx
- Uncroppedimages.pdf